

ALDOL REACTION – ISOTOPE EFFECTS, MECHANISM AND DYNAMIC  
EFFECTS

A Dissertation

by

MATHEW J. VETTICATT

Submitted to the Office of Graduate Studies of  
Texas A&M University  
in partial fulfillment of the requirements for the degree of

DOCTOR OF PHILOSOPHY

December 2009

Major Subject: Chemistry

ALDOL REACTION – ISOTOPE EFFECTS, MECHANISM AND DYNAMIC  
EFFECTS

A Dissertation

by

MATHEW J. VETTICATT

Submitted to the Office of Graduate Studies of  
Texas A&M University  
in partial fulfillment of the requirements for the degree of

DOCTOR OF PHILOSOPHY

Approved by:

Chair of Committee, Daniel A. Singleton  
Committee Members, Brian T. Connell  
Frank M. Raushel  
Thomas K. Wood  
Head of Department, David H. Russell

December 2009

Major Subject: Chemistry

## ABSTRACT

Aldol Reactions–Isotope Effects, Mechanism and Dynamic Effects.

(December 2009)

Mathew J. Vetticatt, B.Tech., UICT, Mumbai

Chair of Advisory Committee: Dr. Daniel A. Singleton

The mechanism of three important aldol reactions and a biomimetic transamination is investigated using a combination of experimental kinetic isotope effects (KIEs), standard theoretical calculations and dynamics trajectory simulations. This powerful mechanistic probe is found to be invaluable in understanding intricate details of the mechanism of these reactions. The successful application of variational transition state theory including multidimensional tunneling to theoretically predict isotope effects, described in this dissertation, represents a significant advance in our research methodology.

The role of *dynamic effects* in aldol reactions is examined in great detail. The study of the proline catalyzed aldol reaction has revealed an intriguing new dynamic effect – quasiclassical corner cutting – where reactive trajectories cut the corner between reactant and product valleys and avoid the saddle point. This phenomenon affects the KIEs observed in this reaction in a way that is not predictable by transition state theory. The study of the Roush allylboration of aldehydes presents an example where recrossing affects experimental observations. The comparative study of the allylboration of two electronically different aldehydes, which are predicted to

have different amounts of recrossing, suggests a complex interplay of tunneling and recrossing affecting the observed KIEs.

The Mukaiyama aldol reaction has been investigated and the results unequivocally rule out the key carbon-carbon bond forming step as rate-limiting. This raises several interesting mechanistic scenarios – an electron transfer mechanism with two different rate-limiting steps for the two components, emerges as the most probable possibility. Finally, labeling studies of the base catalyzed 1,3-proton transfer reaction of fluorinated imines point to a stepwise process involving an azomethine ylide intermediate. It is found that dynamic effects play a role in determining the product ratio in this reaction.

## DEDICATION

To the three people who have made me who I am – my Mom, my Dad and my wife

## ACKNOWLEDGEMENTS

I would like to thank my advisor, Dr. Daniel A. Singleton, for his patience, guidance and support throughout the course of this research.

I would also like to thank the past and present members of the Singleton research group for their invaluable contributions to my work, the stimulating conversations and their expert guidance.

Finally, I would like to thank my family – Jen, Billy and Katharina – for supporting me through the rough times and for sharing my moments of success.

## TABLE OF CONTENTS

	Page
ABSTRACT .....	iii
DEDICATION .....	v
ACKNOWLEDGEMENTS .....	vi
TABLE OF CONTENTS .....	vii
LIST OF FIGURES.....	x
LIST OF TABLES .....	xi
CHAPTER I INTRODUCTION .....	1
1.1 Transition State Theory and Kinetic Isotope Effects .....	2
1.2 Experimental KIE Measurements .....	3
1.3 Theoretical Prediction of KIEs.....	6
1.4 Dynamic Effects in Ordinary Organic Reactions.....	7
CHAPTER II CORNER CUTTING IN ORGANOCATALYSIS .....	10
2.1 The Manz Phenomenon.....	10
2.2 Organocatalyzed Aldol Reactions .....	12
2.3 Experimental KIEs .....	15
2.4 Mechanistic Models .....	19
2.5 Predicted KIEs.....	24

	Page	
2.6 Trajectory Studies .....	26	
2.7 Discussion and Conclusion .....	31	
CHAPTER III BASE CATALYZED ISOMERIZATION OF FLUORINATED		
IMINES.....	33	
3.1 Transamination.....	33	
3.2 Results from Labeling Studies .....	36	
3.3 Theoretical and Dynamics Trajectory Calculations .....	41	
3.4 Discussion and Conclusion .....	45	
CHAPTER IV DYNAMIC EFFECTS IN THE ROUSH ALLYLBORATION OF		
ALDEHYDES .....	47	
4.1 Introduction .....	47	
4.2 Exploratory Theoretical Studies.....	49	
4.3 Experimental KIEs .....	53	
4.4 Theoretical Structures and KIEs from TST.....	55	
4.5 Qualitative Effects of Recrossing.....	58	
4.6 Variational TST Predictions.....	60	
4.7 Discussion and Conclusions.....	61	
CHAPTER V MECHANISM OF MUKAIYAMA ALDOL REACTION.....		62
5.1 Directed Aldol Reactions .....	62	
5.2 Experimental KIEs .....	65	



	Page
5.3 Theoretical Models.....	69
5.4 Theoretical KIEs .....	75
5.5 Discussion and Conclusion .....	76
CHAPTER VI EXPERIMENTAL PROCEDURES.....	81
6.1 General Calculational Procedures. ....	81
6.2 Experimental Procedures for ‘Corner Cutting in Organocatalysis’ .....	86
6.3 Experimental Procedures for ‘Base catalyzed isomerization of fluorinated imines’ .....	91
6.4 Experimental Procedures for ‘Dynamic Effects in the Roush Allylboration of Aldehydes’ .....	93
6.5 Experimental Procedures for ‘Mechanism of Mukaiyama Aldol Reaction’ ..	95
CHAPTER VII CONCLUSION .....	99
REFERENCES.....	102
VITA.....	109

## LIST OF FIGURES

	Page
Figure 1. The origin of a kinetic isotope effect .....	3
Figure 2. 2-D representation of the Manz corner cutting phenomenon .....	12
Figure 3. (a) Relative $^{13}\text{C}$ isotopic composition in the aldol product 11. (b) The corresponding intramolecular $^{13}\text{C}$ KIE. Standard deviations are shown in parenthesis.....	16
Figure 4. Experimental intermolecular $^{13}\text{C}$ KIEs ( $k_{12\text{C}}/k_{13\text{C}}$ ) of the proline catalyzed aldol reaction of acetone and <i>o</i> -chlorobenzaldehyde. The three sets of KIEs represent three independent experiments and the standard deviations of these measurements are indicated in parentheses. The isotopic composition of the carbons derived from acetone is not meaningful in this experiment.....	18
Figure 5. 2D analytical potential energy surface for the key step in proline catalyzed aldol reaction.....	26
Figure 6. 2D trajectories propagated from the area of 25 .....	29
Figure 7. Potential energy surface for the proline-catalyzed aldol reaction, along with sample quasiclassical trajectories. Smooth lines are 2-D trajectories on the analytical surface and knobby lines are trajectories in 87 dimensions on the B3LYP/6-31G*/PCM surface. ....	30
Figure 8. Potential energy (black) and Free energy (blue) paths for the reaction of (a) <i>p</i> -nitrobenzaldehyde and (b) <i>p</i> -anisaldehyde.....	58
Figure 9 Experimental KIEs for (a) <i>p</i> -tolualdehyde and (b) pinacolone – $^{13}\text{C}$ KIEs are in black and the $^2\text{H}$ KIEs are in red The two sets of KIEs represent two independent experiments and the standard deviations of these measurements ( $n = 6$ ) are indicated in parentheses.....	66

## LIST OF TABLES

	Page
Table 1. Experimental and predicted KIEs for proline-catalyzed aldol reactions.....	24
Table 2. Key bond lengths for transition state 26 at various levels of theory.....	28
Table 3. Results from labeling studies in $d_4$ -methanol/methanol.....	38
Table 4. Results from labeling studies in $d_6$ -benzene .....	40
Table 5. Results from quasiclassical trajectory studies (B3LYP/6-31G*).....	50
Table 6. Experimental intermolecular $^{13}\text{C}$ KIEs ( $k_{12\text{C}}/k_{13\text{C}}$ ) for the reaction of tartrate modified allyl boronates and aromatic aldehydes. The three sets of KIEs for p-nitrobenzaldehyde and two sets for p-anisaldehyde represent independent experiments and the standard deviations of these measurements are indicated in parentheses.....	55
Table 7. Comparison of experimental KIEs for allylboration with KIEs predicted from conventional TST with a one-dimensional tunneling correction.....	57
Table 8 Predicted KIES for allylboration of 44a/b without tunneling.....	59
Table 9. KIE predictions using the rate calculation program POLYRATE.....	61
Table 10. KIE predictions for transition structures 51-58. Highlighted in red are the experimental KIEs (provided for comparison) and the predicted KIEs of theoretical models that best fit experiment. ....	76

## CHAPTER I

### INTRODUCTION

In the mid 1990's, the Singleton group developed methodology for the measurement of kinetic isotope effects (KIEs) at natural abundance.<sup>1</sup> This methodology was initially used in a conventional way for the elucidation of reaction mechanisms. With the increasing availability of relatively accurate calculational methods, a combined experimental and theoretical approach was found to be extremely powerful in mechanistic studies.<sup>2,3</sup> Theoretical methods based on transition state theory (TST) in conjunction with experimental KIEs were successfully employed to gain insight into the transition state geometry and hence the mechanism of several important organic reactions.<sup>2</sup>

Within the framework of conventional TST, the free energy of the transition state is directly related to the reaction rate as described in eq 1.1.<sup>4</sup> Selectivity observed in reactions is associated with relative free energies of competing transition states, with the preferred product in a reaction arising from the lower-energy transition state. Catalysis is explained in terms of lowering of the energy of the transition state relative to that of the uncatalyzed reaction. In short, TST has formed the basis of our understanding of how reactions work.

$$k = \kappa \frac{\mathbf{k}T}{h} e^{-\Delta G_{act}^0/RT} = \kappa \frac{\mathbf{k}T}{h} e^{-\Delta H_{act}^0/RT} e^{\Delta S_{act}^0/R} \quad (1.1)$$

---

This dissertation follows the style of *Journal of the American Chemical Society*.

During the course of rigorous application of the Singleton methodology combining isotope effects and theoretical studies, the Singleton group encountered several instances where conventional TST fails to account for experimental observations.<sup>3,5</sup> When an experimental observation cannot be accounted for within the standard theoretical framework of TST, more detailed examination of the reaction dynamics is required. In the past five years, our research efforts have been directed largely towards the observation and interpretation of phenomena outside of TST that affect kinetic observations in organic reactions.

### **1.1 Transition State Theory and Kinetic Isotope Effects**

Kinetic isotope effect measurements are powerful mechanistic probes. Figure 1 is a 2D representation of the vibrational normal modes associated with the reactant and the transition state for a reaction, focusing on as an example the stretching vibration of a C-H bond. Isotopic substitution, in this case by deuterium, affects the zero-point energy (ZPE) of the vibrational normal modes of a molecule. The main origin of KIEs lies in how the ZPE is different at the stage of reactants versus the transition state. When the normal modes are looser at the transition state versus the starting material, as is most common, the ZPE is decreased and lighter isotopes encounter a smaller barrier. As a result, lighter isotopes tend to react faster ( $k_{\text{light}}/k_{\text{heavy}} > 1$ ) and this observation is referred to as a “normal” isotope effect. Sometimes the normal modes are tighter at the transition state versus the starting material; this causes the ZPE to be increased at the transition state and heavier isotopes encounter a lower barrier. The resulting faster rate

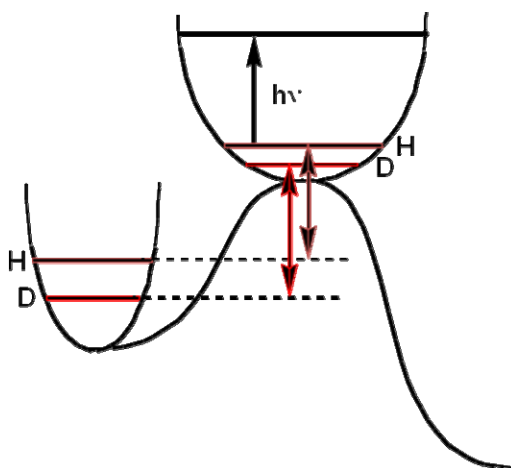


**Figure 1.** The origin of a kinetic isotope effect

for the heavier isotope ( $k_{\text{light}}/k_{\text{heavy}} < 1$ ) is an “inverse” isotope effect. Since the KIEs are intimately associated with the normal modes at the transition state, KIEs can be used to experimentally probe the transition state geometry, i.e. the extent of bond formation / bond breaking occurring as the reaction goes over the transition state.

## 1.2 Experimental KIE Measurements

Since KIEs are rate differences observed when a molecule is replaced by an isotopologue, it might be thought that isotope effects may be measured by a direct measurement of rate constants. This is often done when the rate differences are large. The imprecision in the measurement of rate constants makes their use in the measurement of small KIEs impractical in most cases. As a result, small KIEs are measured in competition reactions that rely on the precise measurement of the isotopic

composition of either starting materials or products. These competition reactions were traditionally carried out using labeled materials. The methodology developed in the Singleton research group allows these measurements to be made at natural abundance.

The Singleton method for the determination of  $^{13}\text{C}$  KIEs at natural abundance has been well documented in papers and dissertations,<sup>1,2</sup> and the discussion here will simply outline the methodology. Each individual carbon and hydrogen in an organic molecule contains at natural abundance approximately 1.1% of  $^{13}\text{C}$  and 0.015% of  $^2\text{H}$ . As a reaction progresses, the starting materials are enriched in the slower reacting isotopomers (isotopically substituted isomers) and the products in the faster reacting ones. If this isotopic enrichment at every position in a molecule can be measured, KIEs can be determined without the use of explicitly labeled substrate. In this dissertation, this idea is applied in three different ways to determine  $^{13}\text{C}$  and  $^2\text{H}$  KIEs at natural abundance.

(a) *Intermolecular starting material KIEs* – The original methodology developed in the Singleton group measured KIEs by analysis of starting material recovered from reactions taken to high conversion, typically ~80%. The isotopic composition of this recovered material is determined by NMR at natural abundance and compared to that of unreacted starting material (drawn from the bottle originally used for the reaction). The enrichment (depletion) thus measured can be used to determine the KIEs based on eq 1.2, where  $F_1$  is the fractional conversion of the lighter isotopomer and  $R/R_0$  is the proportion of minor isotopic component in recovered starting material versus the original material.

$$\log(1 - F_1) / \log[(1 - F_1)(R / R_0)] \quad (1.2)$$

This methodology has some advantages when it can be applied. One advantage is that the precision of the KIEs obtained can exceed the precision of the analysis. Another advantage is that the KIEs are insensitive to further side reactions that the product may undergo. A disadvantage is that the methodology cannot be applied to reactants that must be used in large excess.

- (b) *Intermolecular product KIEs* – An alternative process involves taking reactions to low conversion (typically ~20%) and analyzing the isolated reaction product. The isotopic composition of the product is compared to that of product isolated from a reaction taken to 100% conversion reaction. Equation 1.3 is then used to calculate the KIEs. This method is prone to two possible errors.

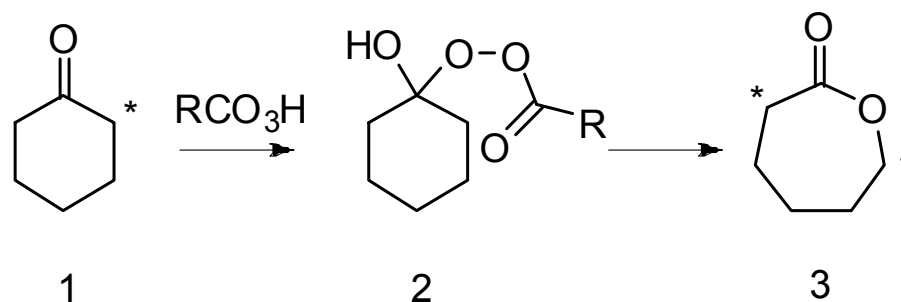
$$\log(1 - F_1) / \log[1 - (F_1 * R_p / R_0)] \quad (1.3)$$

Further conversion of product to form side product will adversely affect the measurement. Also, errors may arise from any inefficiency in the ‘100% conversion’ reaction. In this dissertation, a method to address at least one of these sources of error is discussed.

- (c) *Intramolecular product KIEs* – While intermolecular KIEs in general relate to the *rate-limiting step* of a reaction, intramolecular KIE measurements are elegant probes that provide valuable information about intermediates and subsequent steps in a reaction. For example, in the Baeyer-Villiger oxidation of **1**, the rate



determining step is the formation of the hemiperacetal **2**. When partially labeled **1** (assume \* is a  $^{13}\text{C}$  label) passes through a rate-limiting



transition state and has a regiochemical choice of reactive isotopes, the product distribution (i.e. where the label actually ends up in **3**) reflects the KIE of the second step. This information can be gained by analyzing the  $^{13}\text{C}$  composition of product isolated from this reaction. The intramolecular product KIE measured represents the KIE of the “product determining step” of a reaction, that is, the first step that irreversibly desymmetrizes a symmetric molecule.<sup>6</sup> Used in conjunction with intermolecular KIEs, intramolecular KIEs can be used to distinguish a single step from a multi-step reaction mechanism.

### 1.3 Theoretical Prediction of KIEs

Computational studies can predict in complete detail the mechanisms of chemical reactions. However, it must be remembered that the computations employed in quantum chemistry are themselves only approximate models of electronic structure in reality, and

systems being modeled are usually only crude models of complex reactions including solvent. As a result, the key question in computational studies is whether the results obtained are accurate depictions of the experimental chemistry. The Singleton group uses a comparison of the experimental KIEs with predicted KIEs to gauge the accuracy of the calculations and interpret the experimental isotope effects.

The process of predicting KIEs uses density functional theory (DFT) or ab initio calculations to locate transition structures for the experimental system. Solvent models are incorporated into our calculations when deemed necessary. After considering the strengths and weaknesses of computational methods as well as their practicality, a method is chosen for a system of interest. This calculational method is then used to predict KIEs for a variety of mechanistic possibilities. This is done from scaled theoretical vibrational frequencies using conventional transition state theory by the Bigeleisen and Mayer method.<sup>7</sup> Tunneling corrections are then applied to the computed KIEs using a one-dimensional infinite parabolic barrier model.<sup>8</sup> In this dissertation, we have also started to make use of more advanced versions of TST to predict KIEs, including variational transition state theory (VTST) with the inclusion of multidimensional tunneling.<sup>9</sup>

#### **1.4 Dynamic Effects in Ordinary Organic Reactions**

The products and selectivities of some organic reactions cannot be explained within the normal framework of reaction barriers and transition state theory. In these cases, explicit consideration of the detailed motions and momenta of the atoms can often

rationalize the experimental results.<sup>10</sup> Such reactions may be described as involving "dynamic effects." The recognition of the breadth of reactions involving dynamic effects and the detailed understanding of experimental observations in these reactions remains a substantial challenge in chemistry.

Dynamic effects can arise in several ways. In reactions involving "dynamic matching", the selectivity after passing through a shallow intermediate is related to the momentum of atoms crossing an initial transition state.<sup>11,12,13</sup> Other reactions involve "bifurcating energy surfaces," in which reactions that pass through a rate-limiting transition state can proceed downhill to two or more products.<sup>14,15,16,17,18</sup> A third dynamic effect involves the recrossing of barriers; much recrossing is predictable and handled well by variational transition state theory, but some recrossing is not readily predictable statistically,<sup>19</sup> and such "non-statistical recrossing" can affect observations in organic reactions.<sup>20</sup> Reactions can involve a complex combination of dynamic effects.<sup>5,20</sup> Chapters III and IV of this dissertation describe two examples where dynamic effects impact experimental observations.

We have recently come across yet another type of dynamic effect that we believe has relevance to many organic and enzymatic reactions. The effect arises in reactions where heavy atom bonding changes are accompanied by a proton transfer, which encompasses almost all of general acid/base catalysis. In such case trajectories deviate from the minimum energy path (MEP) by cutting the corner between reactant and product valleys, bypassing the transition state. This phenomenon occurs well above reaction threshold energies and is a consequence of the large ZPE of heavy atom-hydrogen bonds. The first

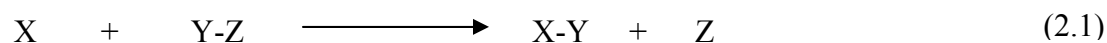
experimental example of this new type of dynamic effect, in a topical organic reaction, is described in Chapter II.

CHAPTER II  
CORNER CUTTING IN ORGANOCATALYSIS

### 2.1 The Manz Phenomenon

Dynamic effects exist because statistical rate theories such as TST and RRKM<sup>21</sup> (Rice–Ramsperger–Kassel–Marcus) theory are simplified models for understanding reactivity. These models are used ubiquitously, precisely because they are simple, but still useful for most reactions. It is well understood, at least in the physical chemistry literature, that the rates of chemical reactions are ultimately governed by quantum dynamics.<sup>22</sup> This understanding in fact predates Eyring’s transition state theory.<sup>4</sup>

The simplest non-trivial reactions involve the collision of atoms with diatomics to effect a substitution of one atom with another (eq 2.1). The consideration of such

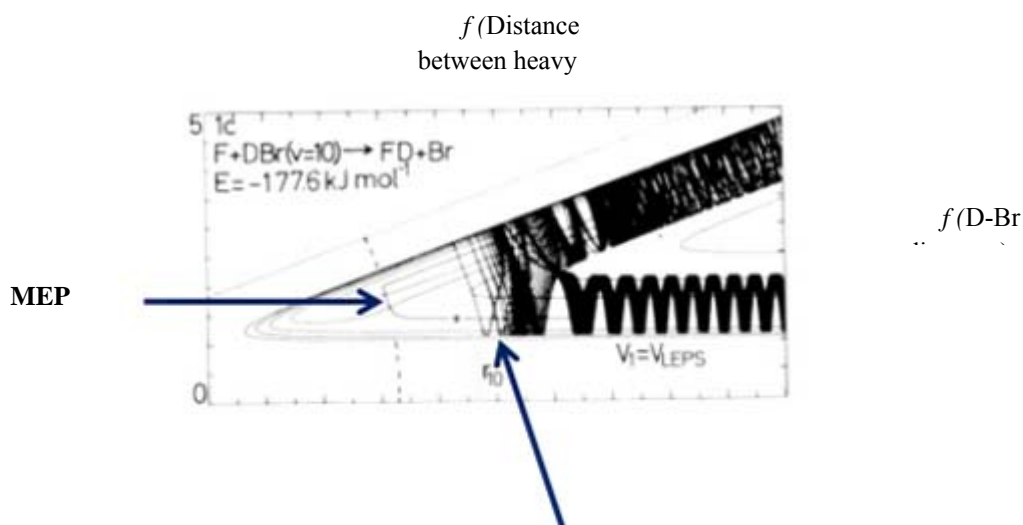


“triatomic” collisions can be limited to the collinear case reducing the potential energy surface to two dimensions (plus energy).<sup>23</sup> The simplicity of triatomic collisions has led to their extensive study in classical-dynamical and quantum-dynamical studies of reaction rates. Such studies have often shown that the rates of chemical reactions involve factors not considered in conventional TST, for example recrossing and tunneling.<sup>9</sup> It can be unclear, however, whether an interesting observation in a triatomic collision is relevant to more complex reactions. For this reason, some of the more intriguing results

from triatomic studies have been largely ignored. Such is the case of a phenomenon predicted by Manz. Building on earlier work of Parr and Polanyi,<sup>24</sup> Manz theoretically predicted in 1988 that quasiclassical trajectories could deviate strongly from the MEP and shortcut, without tunneling, potential-energy saddle points in passing from reactant to product valleys.<sup>25</sup> Manz theoretically studied the collinear hydrogen transfer reaction of fluorine atoms with two isotopic variants of hydrogen bromide as described in eq 2.2.



Classical trajectory simulations of these reactions revealed the fascinating observation that very few trajectories passed near the region of the saddle point. As shown in Figure 2,<sup>25</sup> at large fluorine-bromine distances (x-axis), the ZPE in the D-Br or Mu-Br bond carries the trajectories from the starting-material valley to the product valley, ‘cutting the corner’ of the MEP. It is important to recognize that this phenomenon is distinct from tunneling (which can be described as corner cutting through the reaction barrier below threshold energies) and the occurrence of one does not imply or exclude the other. The extent of deviation from the MEP depends on the mass of the light atom; muonium corner cuts more than deuterium. This intriguing phenomenon has been largely ignored.



### Corner Cutting Trajectories

**Figure 2.** 2-D representation of the Manzhong corner cutting phenomenon

We envisioned that this phenomenon might have broader significance. Reactions involving a combination of heavy-atom bonding changes and proton transfer are quite common, the largest class being general acid- and base-catalyzed reactions. We chose to study the topical proline catalyzed aldol reaction as a prototype of an organic reaction that might exhibit this novel phenomenon.

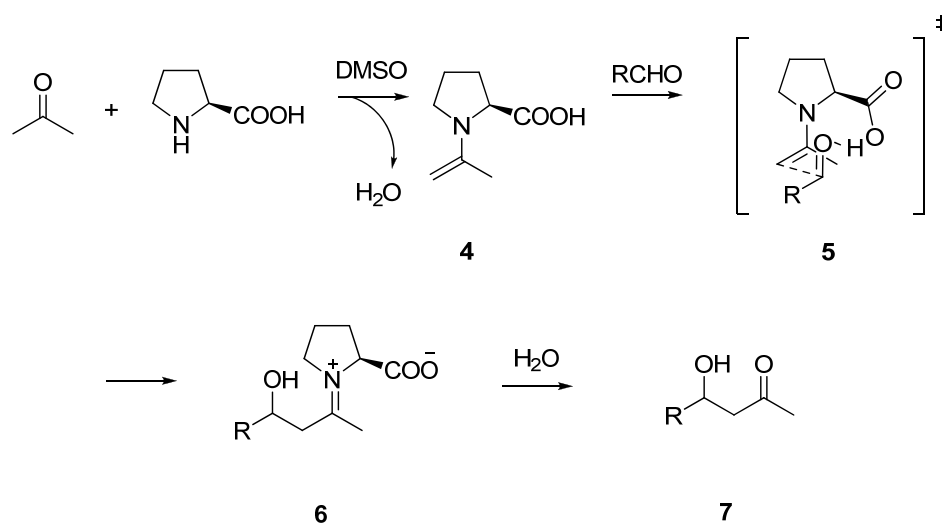
## 2.2 Organocatalyzed Aldol Reactions

Organocatalysis has emerged as an important approach to asymmetric synthesis. Aldol reactions mediated by proline and related molecules are a major category of organocatalytic reactions, and initial intramolecular examples were demonstrated over 30 years ago.<sup>26</sup> However, the broad potential of these reactions was only established in

recent years by the demonstration of efficient and highly enantioselective intermolecular variants.<sup>27</sup>

Experimental mechanistic studies of these reactions, including  $^{18}\text{O}$  incorporation<sup>28</sup> and ESI-MS<sup>29</sup> (Electrospray Ionization Mass Spectrometry) studies have provided evidence for an enamine-mediated mechanism of the general type shown in Scheme 1. Under conditions appropriate for mechanistic study, List has shown that there is only one proline molecule involved in the mechanism of this reaction.<sup>30</sup> It should be noted that the commonly observed nonhomogeneity of these reactions can complicate observations, while demonstrating novel stereochemical principles.<sup>31</sup>

**Scheme 1**

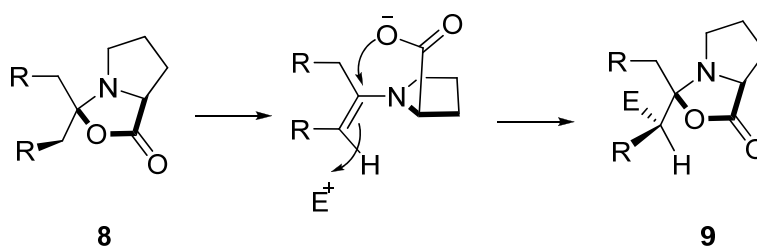




Theoretical calculations by Houk and List support a stereochemistry-determining transition state resembling **5** involving the anti enamine **4**. In this structure, proton transfer from the carboxylic acid to the incipient alkoxide derived from the aldehyde accompanies the carbon-carbon bond formation, and the combination of the two processes is considered critical in determining the favored stereoisomer.<sup>32</sup> The stereochemical outcome of the reaction in several cases fits well with calculations based on this mechanistic model, but otherwise the experimental support for this transition state and many features of the reaction mechanism is minimal.

The mechanistic model of Scheme 1 has recently been questioned by Seebach and Eschenmoser.<sup>33</sup> In the Seebach/Eschenmoser model, the product-determining step is viewed as an electrophilically induced  $\gamma$ -lactonization on the *syn* enamine, as in the conversion of **8** to **9** in Scheme 2. The process would account for the observation of oxazolidinones as initial products in some proline-catalyzed reactions, and the product stereochemistry could be rationalized as affording the most stable bicyclic oxazolidinone **9**. This mechanism has not seen explicit experimental or calculational scrutiny.

### Scheme 2



We undertook a combined experimental and calculational study of the proline catalyzed aldol reaction of acetone with aromatic aldehydes. Our initial goal in this study was to distinguish between the mechanistic proposals above and provide an experimental basis for key aspects of the mechanism and the stereochemistry-determining step of the reaction. In the process, however, the intriguing experimental observations associated with reactions involving simultaneous heavy-atom motion and proton transfer became apparent, and we investigated the importance of the Manz phenomenon to rate and enantioselectivity of the reaction.

### 2.3 Experimental KIEs

The prototypical proline catalyzed reaction of acetone with aromatic aldehydes was chosen for study of the  $^{13}\text{C}$  isotope effects employing NMR methodology at natural abundance.<sup>1</sup> Due to complications in the NMR analysis, slightly different systems were



used to determine the intramolecular and intermolecular  $^{13}\text{C}$  KIEs. In a scaled up analog of standard experimental conditions,<sup>27</sup> the reaction of *p*-nitrobenzaldehyde (**10**) and acetone proceeded cleanly to afford a product mixture consisting of 92% of **11** along with small amounts of elimination and double aldol products. This reaction is not suitable for the study of the intermolecular  $^{13}\text{C}$  KIEs for reaction of the acetone in a

standard way,<sup>1</sup> since acetone is used in large excess (30 equiv). However, analysis of the <sup>13</sup>C isotopic composition at C1 versus C3 of the aldol product **11**, under conditions optimal for obtaining relative integrations within a single spectrum,<sup>6,20,34</sup> provides at natural abundance a direct measurement of the intramolecular isotope effect. In the numerical interpretation of these integrations, it was necessary to take into account the fact that C3 is subject to two <sup>1</sup>J <sup>13</sup>C-<sup>13</sup>C couplings with satellites not included in the integration range, while C1 is subject to only one such satellite coupling. To allow for this the integration of C3 was adjusted by the 0.0107(8) natural abundance of <sup>13</sup>C. Figure 3a shows the resulting relative <sup>13</sup>C isotopic composition of C1 versus C3 based on the corrected integrations. The intramolecular <sup>13</sup>C KIE, as  $k_{12C}/k_{13C}$ , is the reciprocal of the relative <sup>13</sup>C composition and is shown in Figure 3b.

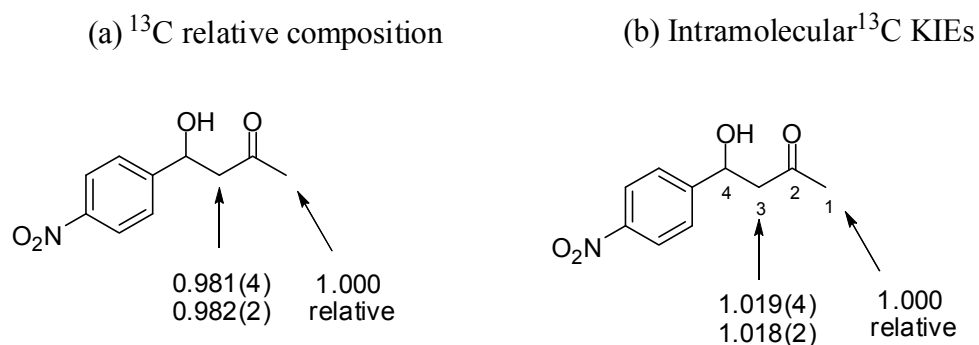
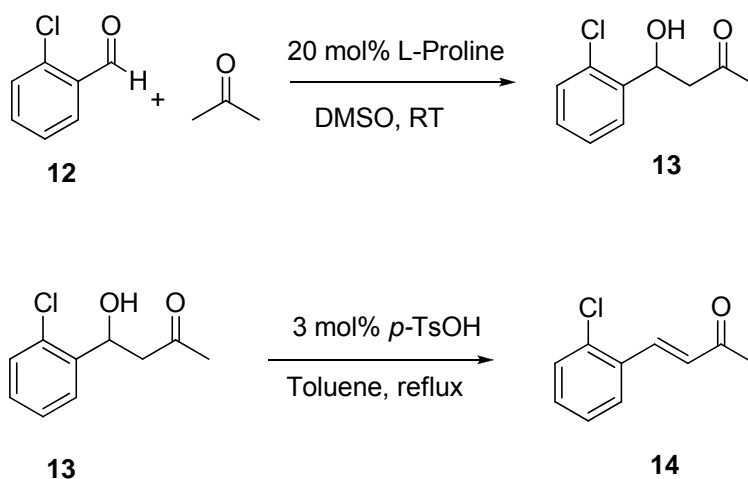


**Figure 3.** (a) Relative <sup>13</sup>C isotopic composition in the aldol product **11**. (b) The corresponding intramolecular <sup>13</sup>C KIE. Standard deviations are shown in parenthesis.

For determining the *intermolecular* <sup>13</sup>C KIEs for the aldehyde in these reactions, the proline-catalyzed reaction of acetone with *o*-chlorobenzaldehyde (**12**) was studied. The

reaction of **12** and acetone afforded product **13** in 95% yield. Reactions were taken to  $20 \pm 2\%$ ,  $26 \pm 2\%$  and  $11 \pm 2\%$  conversion, and the product was dehydrated quantitatively to **14** by treatment with catalytic amounts of *p*-TsOH.



The  $^{13}\text{C}$  composition of these samples was compared to samples of **14** obtained from 100% conversion reactions. The peak for C6' of **14** was used as a standard in the NMR analysis with the assumption that the isotopic composition in this position was unchanged. The resulting intermolecular  $^{13}\text{C}$  KIEs are shown in Figure 4.

The H/D isotope effect was measured from absolute kinetics. The initial nonhomogeneity of proline catalyzed reactions coupled with catalyst destruction in later stages of the reaction precluded kinetic measurements using proline itself. For this reason the soluble proline derivative **15** was synthesized.<sup>35</sup> In exploratory studies, it was found that reactions using 10 mol % of **15** with acetone/*d*<sub>6</sub>-acetone and **10** in DMSO were homogenous and kinetically well behaved to moderate conversions.

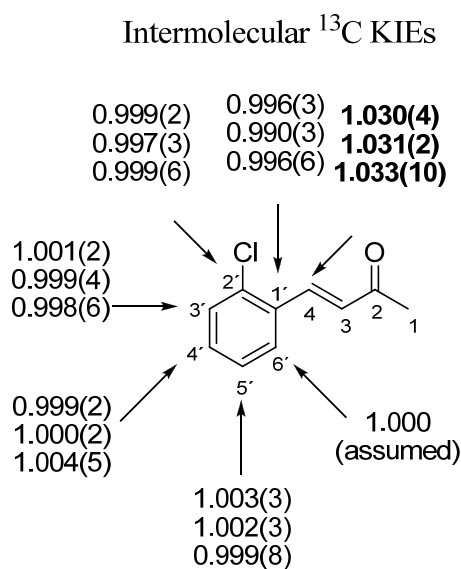
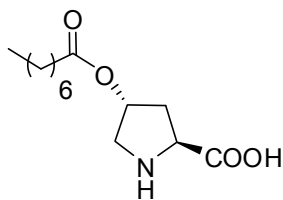


**Figure 4.** Experimental intermolecular  $^{13}\text{C}$  KIEs ( $k_{12\text{C}}/k_{13\text{C}}$ ) of the proline catalyzed aldol reaction of acetone and *o*-chlorobenzaldehyde. The three sets of KIEs represent three independent experiments and the standard deviations of these measurements are indicated in parentheses. The isotopic composition of the carbons derived from acetone is not meaningful in this experiment.

To circumvent the issue of catalyst destruction, we decided to study *initial rates* in order to determine the  $k_{\text{H}}/k_{\text{D}}$  of the reaction. The initial rates for these reactions were followed by pre-equilibrating **15** and acetone/  $d_6$ -acetone in DMSO followed by addition



**15**

of **10** and determination of the conversion by NMR analysis of quenched aliquots. The observed conversions at a series of early points were fit to the assumed rate law: rate =

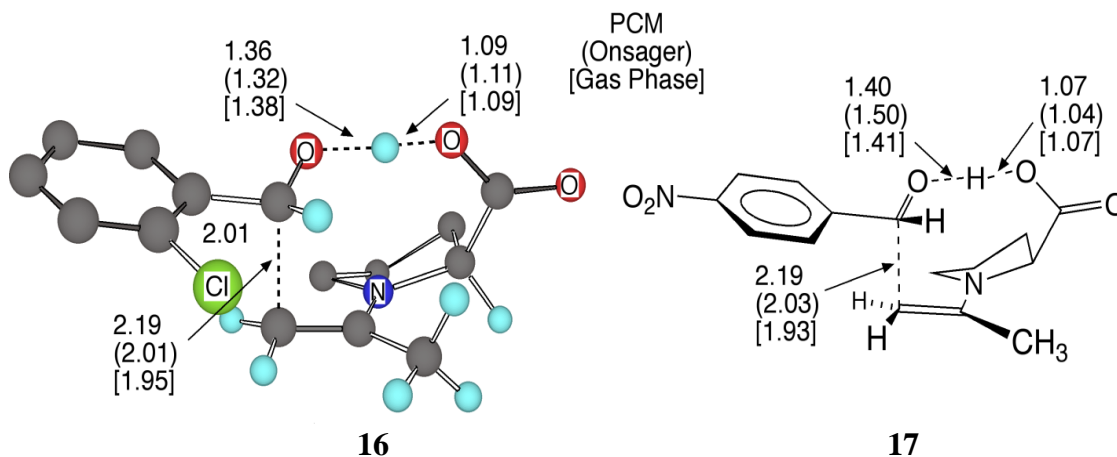
$k_{obs}$  [**15**] [**10**]. The best-fit  $k_{obs}$ 's were  $4.00 \pm 0.40 \times 10^{-2}$  and  $1.51 \pm 0.16 \times 10^{-2} \text{ M}^{-1}\text{s}^{-1}$  for acetone versus acetone- $d_6$ , respectively, giving  $k_H/k_D = 2.6 \pm 0.4$ . In a second set of matched reactions, the  $k_{obs}$  was  $3.27 \pm 0.32 \times 10^{-2}$  and  $1.19 \pm 0.11 \times 10^{-3} \text{ M}^{-1}\text{s}^{-1}$ , giving  $k_H/k_D = 2.8 \pm 0.4$ .

## 2.4 Mechanistic Models

We start the process of interpreting the experimental isotope effects by adopting the routine calculational approach of locating saddle points on potential energy surfaces and treating these saddle points within conventional transition state theory. It should be noted at the outset that this process is likely subject to multiple sources of error. A straightforward source of error is with regard to the accuracy of the potential energy surfaces employed, due to both intrinsic limitations in the calculations employed (B3LYP calculations employing a 6-31+G\*\* basis set) and error arising from the substantial difficulty of modeling of the energetic effects of the solvent on a polar reaction in solution. In a later section we will address the critical but more subtle error associated with the application of transition state theory to this reaction involving a combination of heavy-atom and light-atom motion.

The proline catalyzed aldol reaction of acetone with **10** and **12** were explored in B3LYP calculations employing a 6-31+G\*\* basis set and an Onsager solvent model<sup>36</sup> for DMSO, and single-point energies on these structures were obtained at the B3LYP/6-31+G\*\* level using a PCM solvent model<sup>37</sup> and Bondi atomic radii.<sup>38</sup> Structures judged to be important based on their energies were optimized using the PCM solvent model.

### Houk-List model



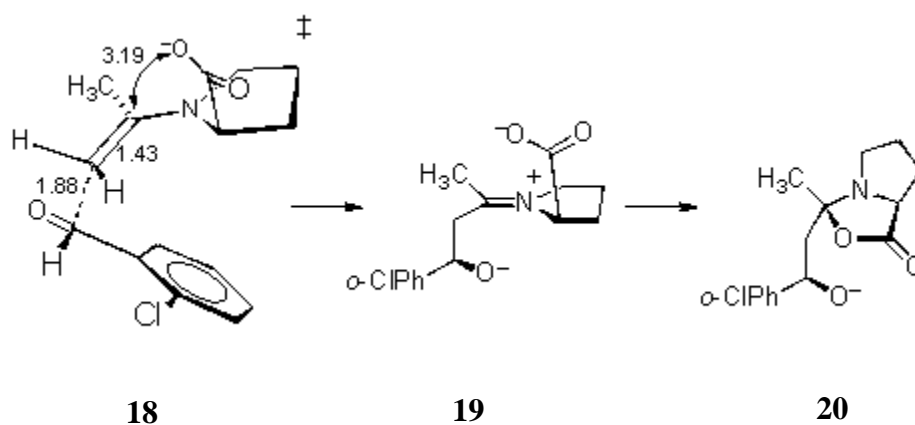
Starting from the earlier closely analogous structures of Houk,<sup>32</sup> transition structure **16** was located for the reaction of **10**. The similar structure **17** was located for the corresponding reaction of **12**. The energetic viability of these transition structures was evaluated using the oxazolidinone derived from proline and acetone **8** (R=H) as the formal resting state of the catalyst. Based on the equilibrium constant of 0.12 for oxazolidinone formation reported by List<sup>28</sup> and the large excess of acetone present in the reaction, the oxazolidinone should be the predominant form taken by the solubilized proline under the reaction conditions here. (As a supporting observation, the rate of the reaction did not change significantly when the concentration of acetone was increased by 50%, as would be expected if the solubilized proline were completely bound to the acetone.) Transition structures **16** and **17** are 12.1 and 10.7 kcal/mol above the starting aldehydes and **8** (R=H) (E + zpe), and in free-energy estimates based on the unscaled harmonic frequencies, the composite  $\Delta G^\ddagger$ 's at a 1 atmosphere standard state would be 25.0 and 23.2 kcal/mol. The latter barrier would correspond to a bimolecular rate

constant of  $0.0015 \text{ M}^{-1}\text{s}^{-1}$ . Considering the limitations of the calculation, the agreement with the rate constant observed above for the reaction mediated by **15** is excellent.

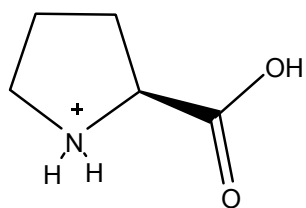
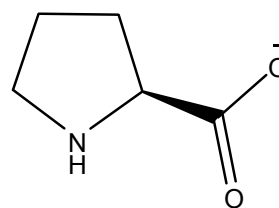
### Seebach/Eschenmoser model

We explored a series of structures in order to provide calculational models for alternative mechanisms and predict the isotope effects expected for these alternatives. As an initial model for the earlier mentioned Seebach/Eschenmoser mechanism, transition structure **18** for the addition of the conjugate base of the enamine of acetone to **12** was located. Seebach and Eschenmoser envisioned this reaction as an electrophilically induced  $\gamma$ -lactonization process, in which the addition of the enamine to the aldehyde was accompanied by a concerted attack of the proline carboxylate on the incipient iminium carbon, minimizing charge separation. No such concerted transition structure could be located. Instead, **18** leads to the carboxylate-iminium-alkoxide triple ion **19**. There is no propensity for the concerted process because the subsequent formation of oxazolidinone **20** by a *5-endo-trig* ring closure faces a significant barrier of 12 kcal/mol and it would be energetically unfavorable to combine the addition and lactonization steps.



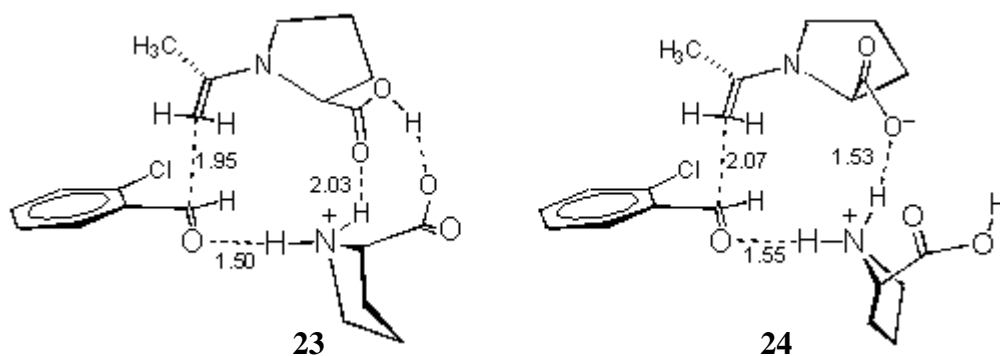


Structure **18** itself appears to be energetically untenable, as in free-energy estimates **18** is 36.9 kcal/mol above that starting **12** and **8** (R=H), assuming the proton released to form the anionic **12** is taken up as a protonated amine (modeled by the protonated proline **21**). The free energy of **12** may also be viewed as being 36.4 kcal/mol above acetone / **4a** / **22** (the conjugate base of proline), but there is likely little of **16** in the reaction mixture – the formation of **21** / **22** from two molecules of proline zwitterion in DMSO is predicted to be 18.1 kcal/mol uphill. (The free energy difference is 11.8 kcal/mol in water based on the water pKa's).

**21****22**

Seebach and Eschenmoser recognized that transition states like **18** were likely to be unfavorable compared to the intramolecular Bronsted-acid activation of the aldehyde inherent in transition structures **16** or **17**. They suggested instead that the reaction environment could provide a corresponding Bronsted-acid catalysis, mediated by either water or proline.

To model the latter, seemingly more likely possibility, transition structures **23** and **24** were located. In these structures, a protonated proline is positioned to stabilize the incipient alkoxide anion arising from addition of the enamine to the aldehyde. As would



be expected, the hydrogen bonding lowers the enthalpic barrier versus **18**, by 4.4 and 2.2 kcal/mol for **23** and **24**, respectively. However, the added molecularity is entropically disadvantageous, so that the calculated free-energy barriers at standard state for **23** and **24** are 45.6 and 47.0 kcal/mol. There is considerable room for error in these calculations, but these insurmountable barriers clearly provide no support for these mechanisms.

## 2.5 Predicted KIEs

The  $^{13}\text{C}$  and  $^2\text{H}$  KIEs based on transition structures **16**, **17**, **18**, **23**, and **24** were predicted using scaled theoretical vibrational frequencies using conventional transition state theory by the Bigeleisen and Mayer method<sup>7</sup> as implemented by the program QUIVER.<sup>39</sup> No tunneling correction was applied for the prediction of the primary H/D isotope effect associated with transition structures **16**, **17**, **23** and **24** - the resulting predictions are likely to be a lower bound compared to what would be obtained with a complete treatment of tunneling and variational transition state effects. The results from the KIE predictions based on TST are presented in Table 1.

**Table 1.** Experimental and predicted KIEs for proline-catalyzed aldol reactions.

System	aldehyde $k_{12\text{C}}/k_{13\text{C}}$	intramolecular C3 / C1	H/D KIE
experimental	1.030(4), 1.031(2), 1.033(10)	1.019(4), 1.018(2)	2.6(4), 2.8(4)
<b>16/ 17</b> (gas phase)	1.039	1.032	1.68
<b>16/ 17</b> (Onsager)	1.038	1.034	1.33
<b>16/ 17</b> (PCM)	1.035	1.032	1.97
<b>18</b>	1.044	1.029	0.73
<b>23</b>	1.046	1.032	1.43
<b>24</b>	1.042	1.032	1.54

From the results above, it is clear that conventional TST fails to accurately predict the KIEs, significantly overpredicting the  $^{13}\text{C}$  KIEs and underpredicting the H/D KIE. A more detailed analysis of the reaction path is necessary to understand the origin of this deviation from conventional TST predictions.

Variational transition state theory (VTST) calculations were performed using GAUSSRATE,<sup>40</sup> which interfaces dynamical rate calculations from POLYRATE, developed by Truhlar and coworkers,<sup>41</sup> and electronic structure methods in Gaussian 03.<sup>42</sup> These calculations were performed at the B3LYP/6-31G\* level of theory with an Onsager solvent model for DMSO. KIEs were determined by comparing the rate constants calculated for the parent system with those containing a  $^{13}\text{C}/^2\text{H}$  at the appropriate positions. The difference in KIEs of the TST predictions and the predictions based on VTST analysis (including a small curvature tunneling correction) for this model system was used as a correction for the KIE predictions for the experimental system.

The KIEs calculated by this method performs slightly better in predicting the experimental results. Due to a drop in the ZPE in the area of the saddle point the variational transition state is earlier – a C-C bond length of 1.97 and an O-H length of 1.07 (versus 1.95 and 1.08 at the saddle point calculated at the same level of theory) . After applying the tunneling correction from the model system to the predictions for the experimental system, the predicted  $^{13}\text{C}$  KIE for the aldehyde is 1.041 and the intramolecular C3/C1 KIE is 1.040. The predicted H/D KIE is 1.69; all these predictions are actually farther from experiment.

## 2.6 Trajectory Studies

Figure 5 shows a two-dimensional analytical potential energy surface modeling the key step in this reaction. This surface was generated by fitting a combination of polynomial and Gaussian functions to B3LYP/6-31G\*/PCM (DMSO) grid points of the potential energy surface of the reaction of acetaldehyde and the enamine of acetone.<sup>43</sup> The critical features of this surface are 1. the minimum-energy path involves mainly heavy-atom motion as the geometry approaches and passes through the saddle point, and 2. the orthogonal O-H stretching-type mode at the saddle point is highly anharmonic,

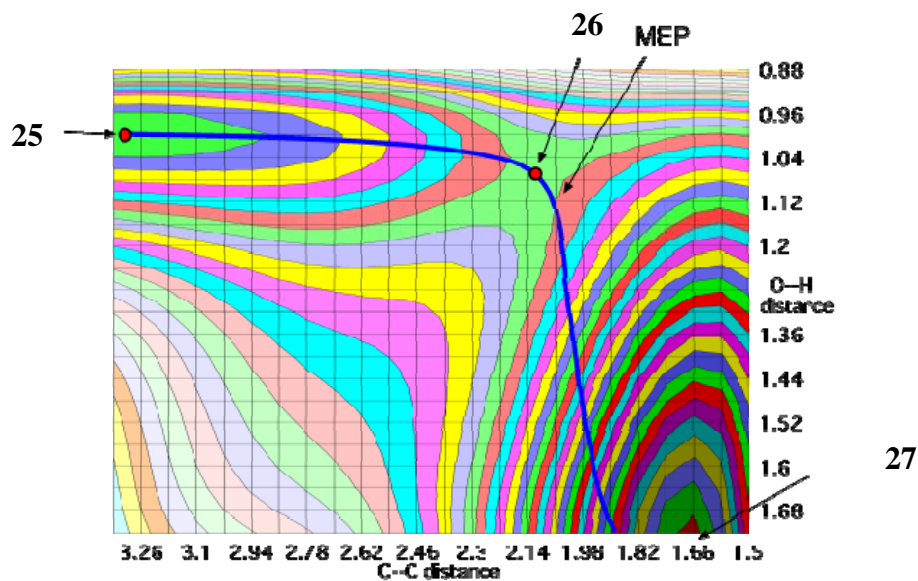
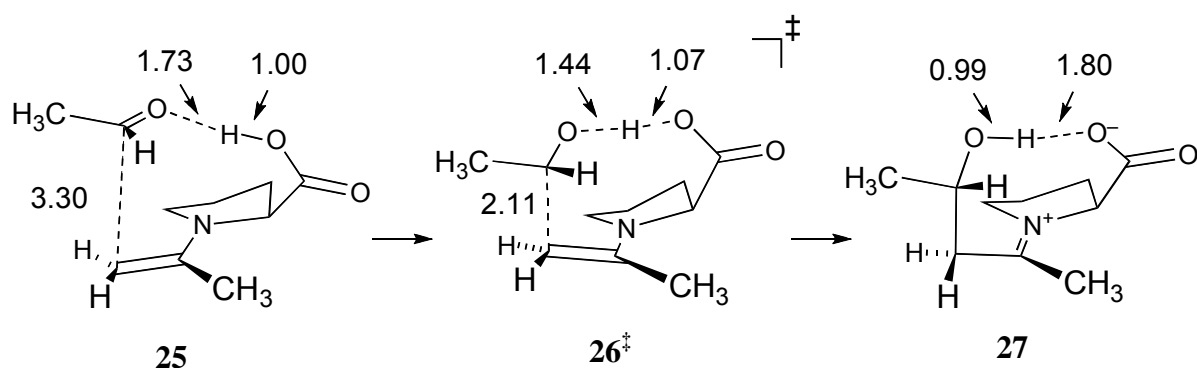


**Figure 5.** 2D analytical potential energy surface for the key step in proline catalyzed aldol reaction



with a rapid rise in energy at shorter O-H distances but a much slower energy gain as the O-H stretches. Structure **25** is the starting-material complex, normally kinetically irrelevant. The saddle point **26<sup>‡</sup>** involves carbon-carbon bond formation accompanied by a very early proton transfer from the carboxylic acid moiety of proline. Structure **27** is the optimized product iminium complex formed from transition state **26<sup>‡</sup>**. A variety of alternative calculational methods, including larger basis sets, gas-phase calculations, and implicit solvent models were explored for this reaction. The key features of the potential energy surface and the stationary points remain essentially unchanged. Table 2 lists the two key distances of the saddle point **26<sup>‡</sup>** for all the calculational methods employed.

Quasiclassical trajectories were initiated on this surface in the area of **25** by giving the O-H vibrational mode its zero-point energy and a random phase and giving the C-C bond-forming mode a random energy based on a classical Boltzmann distribution. Figure 6 shows some typical reactive trajectories. The striking feature of these trajectories is that very few pass through the area of the potential-energy saddle point. Rather, the trajectories show a pronounced propensity to cut the corner between the starting material and product valleys. This is analogous to the observations of Manz for

collinear hydrogen transfer reactions. In 500 trajectories, the mean C-C and O-H distances when crossing the transition state ridge were each 0.15 Å longer than in the saddle point.

**Table 2.** Key bond lengths for transition state **26** at various levels of theory.

<b>Method</b>	<b>C-C length</b>	<b>O-H length</b>
B3LYP/6-31G*	1.89	1.08
B3LYP/6-31+G**	1.97	1.09
B3LYP/6-31+G** Onsager	2.06	1.10
B3LYP/6-31G* PCM	2.11	1.07
mpw1k/6-31G*	1.96	1.04
mpw1k/6-31+G**	2.02	1.04
mpw1k/6-31+G** Onsager	2.10	1.06
mpw1k/6-31+G** PCM	2.21	1.05
M05/6-31G*	1.90	1.04
M05/6-31+G**	2.00	1.03
M05/6-31+G** Onsager	2.07	1.04

This effect can be reproduced in the 87-dimensional space of the real reaction, albeit with some necessary departure from statistical initiation. Trajectories were initiated at **25** in the full system by giving each normal mode its zero-point energy and a random Boltzmann excitation appropriate for 25 °C, plus 8 kcal/mol along a vector aimed from

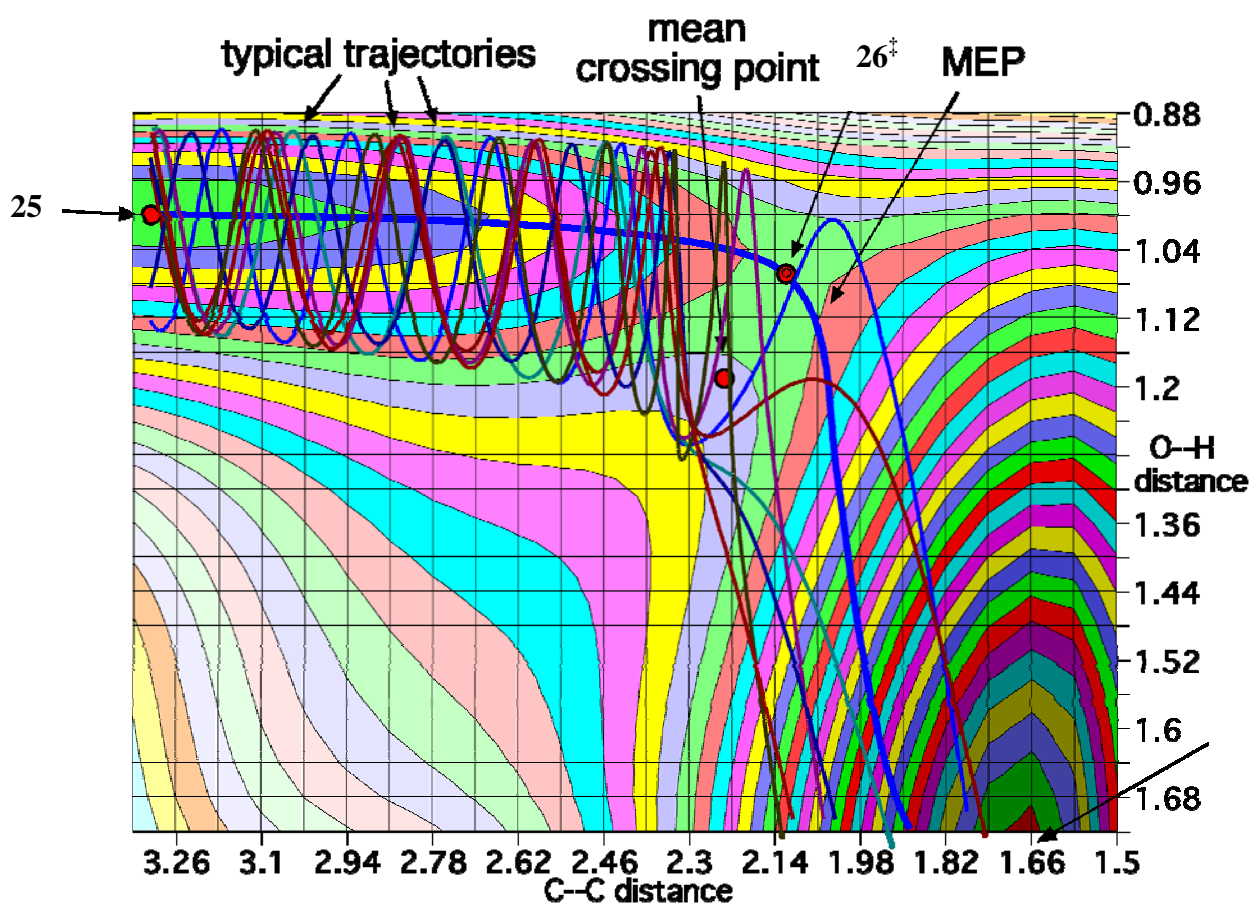


**Figure 6.** 2D trajectories propagated from the area of **25**



**25** toward **26**. The trajectories were then propagated by direct dynamics on the B3LYP/6-31G\*/PCM surface. Very few such trajectories are reactive within a 150 fs time limit, as the excess energy along the vector is partially dissipated into the many degrees of freedom, but reactive trajectories again show pronounced corner cutting.

Figure 7 shows the combined results from all the trajectory studies.

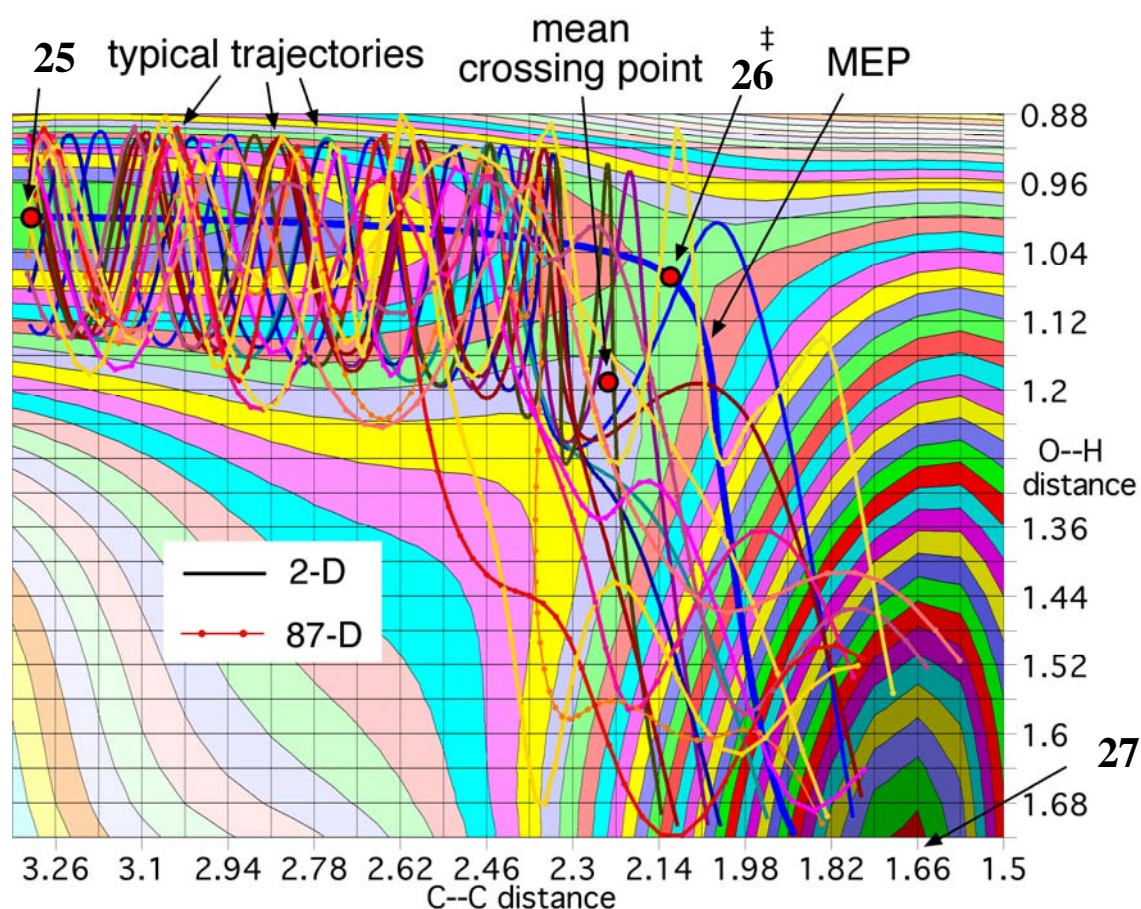


**Figure 7.** Potential energy surface for the proline-catalyzed aldol reaction, along with sample quasiclassical trajectories. Smooth lines are 2-D trajectories on the analytical surface and knobby lines are trajectories in 87 dimensions on the B3LYP/6-31G\*/PCM surface.

It is clear from Figure 7 that majority of the trajectories do not cross the transition state ridge through the potential energy saddle point. The mean crossing point of these quasiclassical trajectories corresponds to a geometry that is earlier along the heavy atom coordinate and significantly later along the light atom coordinate. It is therefore not surprising that the KIEs predicted based on TST or VTST do not resemble the experimental KIEs. An alternative method for calculating KIEs leads to striking results. When the length of the breaking O-H bond is fixed based on the mean crossing point for the trajectories and a TST/SCT prediction is made based on the local curvature at this point, the predicted KIE for the aldehyde carbon is 1.029 and the C3/C1 intramolecular KIE is 1.019. These results are in remarkable agreement with the experimental KIEs and therefore, despite the theoretical shortcomings of this procedure, appear to support the importance of the Manz phenomenon in this system.

## 2.7 Discussion and Conclusion

Comparing our experimental KIE measurements and theoretical KIE predictions of several mechanistic models, the Houk-List model is qualitatively consistent with the experimental KIEs. However KIE predictions based on conventional TST, VTST, and VTST including detailed treatment of tunneling overpredict the intramolecular isotope effect of acetone and underpredict the H/D KIE. The carbonyl KIE is also slightly overpredicted. When a reaction involves a combination of heavy atom motion and light atom transfer at the transition state, trajectories show a pronounced tendency to avoid the transition state and cut the corner between starting material and product valleys. The

consequence of this phenomenon, first proposed theoretically by Manz, is that the experimental KIEs do not reflect the transition state geometry but the point along the transition state ridge that represents the mean crossing point of the quasiclassical trajectories. A longer C-C bond length and a 'more-transferred' hydrogen defines the geometry of this point. The KIEs calculated for this stationary point fits remarkably well with our experimental KIEs.

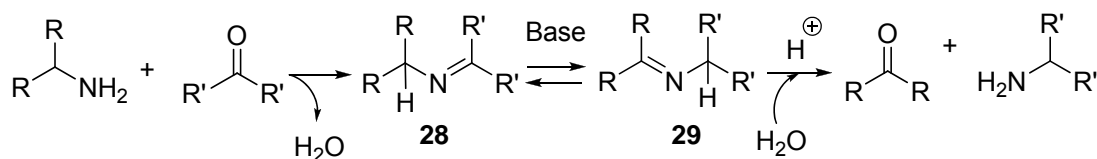
In conclusion, this is the first experimental example of this hitherto unexplored phenomenon in a synthetically useful reaction. We propose that the Manz phenomenon has broader impact than just in this particular example. For any reaction where a proton transfer accompanies heavy atom bonding changes, quasiclassical corner-cutting needs to be considered as a factor that affects the reaction path. This encompasses all of general acid-base catalysis and we believe that this phenomenon will facilitate these reactions. Future work in our group will focus on studying several simple, classical, and well studied examples of general acid-base catalysis that might exhibit the Manz phenomenon which we term as quasiclassical corner-cutting.

## CHAPTER III

## BASE CATALYZED ISOMERIZATION OF FLUORINATED IMINES

**3.1 Transamination**

Biological transamination constitutes a fundamentally important process in living organisms as a pathway of metabolism of  $\alpha$ -keto and  $\alpha$ -amino acids. The overall transamination sequence involves a reversible paired set of reactions in which a primary amine is oxidized to a carbonyl and a carbonyl is reduced to an amine, as shown in Scheme 3. In biological systems, one of the paired reactions is the interconversion of pyridoxamine phosphate and pyridoxal phosphate. The key step in biological

**Scheme 3**

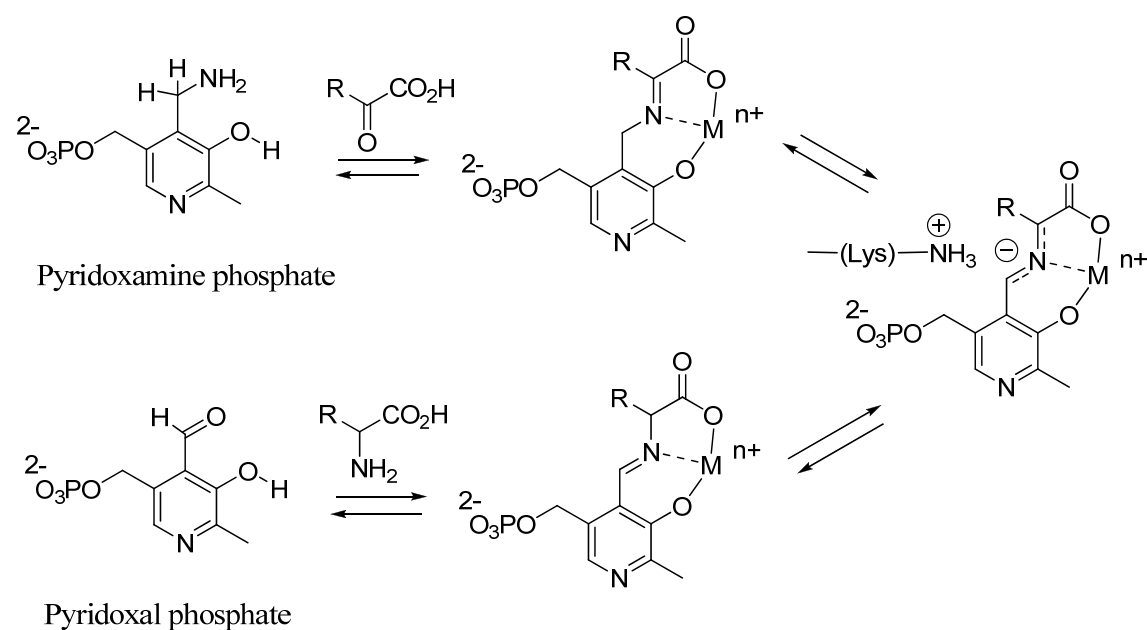
R, R' = Alkyl, Aryl

transamination is a 1,3-proton transfer in adducts of pyridoxamine phosphate with carbonyls (or pyridoxal phosphate with primary amines). In enzymes, this proton transfer is mediated by the  $\alpha$ -amino group of lysine as depicted in Scheme 4.<sup>44</sup>

Mechanistic studies on both the biological as well as model systems have emphasized the importance of metal complex formation as the proton transfer occurs across the

azaallylic system.<sup>45</sup> Cram and coworkers carried out the first studies on the metal-free variant of this reaction – the chemical transamination catalyzed by potassium *t*-butoxide.<sup>46</sup> In this chemical model of the biological transformation, it was found that proton-transfer occurred via a contact ion pair and the isomerization occurred in a suprafacial manner across the face of the delocalized azaallylic carbanion. Because

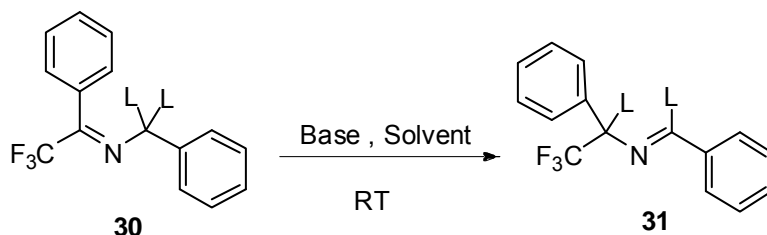
#### Scheme 4



this conversion is an equilibrium process, its efficiency in biological systems depends on coupled reactions. In simple chemical models the equilibrium is not heavily biased and the forward and reverse reactions occur at similar rates. This limits the synthetic utility of the reaction. It also complicates mechanistic studies; many desirable mechanistic

probes such as kinetic isotope effects and labeling studies are most easily employed when there is no reversion of the product to reactants. Such reversion can only be limited when the product is much more stable than the reactants.

A system developed by Soloshonok and coworkers meets this requirement. They have found that the isomerization of imine **30** to **31** can be catalyzed by triethylamine and other weak bases, and that the reaction is virtually irreversible.<sup>47,48</sup> The greater stability of the product in this reaction may be a combination of a steric effect and the destabilizing effect of the electron-withdrawing CF<sub>3</sub> group on the electron-deficient C-N double bond. The Soloshonok system has found synthetic utility, including asymmetric variants<sup>49</sup> and a useful synthesis of  $\alpha$ -fluorinated amines. In this study we take advantage of the irreversibility of the reaction to study the mechanism of the 1,3-proton



transfer. Soloshonok had previously reported that the reaction of **30** mediated by triethylamine as base and carried out in *d*<sub>4</sub>-methanol (1:1:1 molar ratio) resulted in <2% incorporation of deuterium in **31**.<sup>48</sup> The mechanistic proposal based on this observation was that the reaction occurred via a contact ion pair with essentially intramolecular transfer of the proton across the azaallylic system. As we find here, the Soloshonok

results (or at least the interpretations) were not correct. Our results support a much more complicated and interesting mechanism, including a role for dynamic effects.

### 3.2 Results from Labeling Studies

Our initial goal in the study of the conversion of **30** to **31** was to determine if the 1,3-proton transfer was indeed intramolecular as reported by Soloshonok. We studied the isomerization of **30** (L=H) mediated by triethylamine in  $d_4$ -methanol (in an NMR tube) under conditions suitable for NMR analysis (using **30**: base: solvent = 1:2:15). For an intramolecular mechanism, there would be no deuterium incorporation observed in **31**. The deuterium incorporation in **31** was analyzed by comparing  $^1\text{H}$  NMR integrations of the peaks of interest to the integrations of the corresponding peaks in a spectrum of a similar reaction run in protio methanol. Interestingly, we observed ~13% incorporation of deuterium in **31**. This result clearly does not support the proposed mechanism and the 1,3-proton transfer cannot be completely “intramolecular”. In order to study this apparent preference we decided to explore the same reaction using diethylamine – a 2° amine – as the base in this reaction. Under the conditions of our experiment, the amine proton of diethylamine can be assumed to be completely deuterated. After the initial deprotonation of **30**, the protonated diethylamine can protonate the azaallylic anion to give **31** in one of three possible ways i.e. by (i) transferring the proton that it pulled off from **30** (ii) transferring the deuterium that was originally on the diethylamine and (iii) exchanging the proton that it pulled off from **30** with deuterium from the solvent and then transferring one of the deuterons on the protonated amine. Ignoring the third

possibility, and if there was no bias to transfer the proton that it originally pulled off, one would expect to see 50% deuterium incorporation in **31**, assuming there was no isotope effect for the reprotonation. If diethylamine was replaced by a primary amine, say *t*-butylamine, one would expect to see 66% deuterium incorporation in **31**. In our experiments using diethylamine and *t*-butylamine as bases, we observed 23% and 39% deuterium incorporation, respectively.

These results point to a propensity for the amine to return the same proton that it originally pulled off from **30** to the azaallylic anion. However, the deuterium incorporation observed in these reactions is lower than what might be predicted from our statistical analysis. We believe therefore that our experimental observations might in fact be a combination of two factors – a preference to transfer the same proton originally pulled off from **30** and an H/D isotope effect. If there is indeed an H/D KIE, then performing the reaction using **30** (L=D) and an amine in protio methanol should result in a different amount of hydrogen incorporation than deuterium incorporation observed using **30** (L=H) (depending on the magnitude of the KIE). In order to quantify the contribution from the H/D isotope effect, we then conducted the corresponding reverse experiments, i.e., using **30** (L=D) and protio methanol as solvent. The results from the six labeling experiments using methanol as solvent are shown in Table 3.



**Table 3.** Results from labeling studies in  $d_4$ -methanol/methanol.

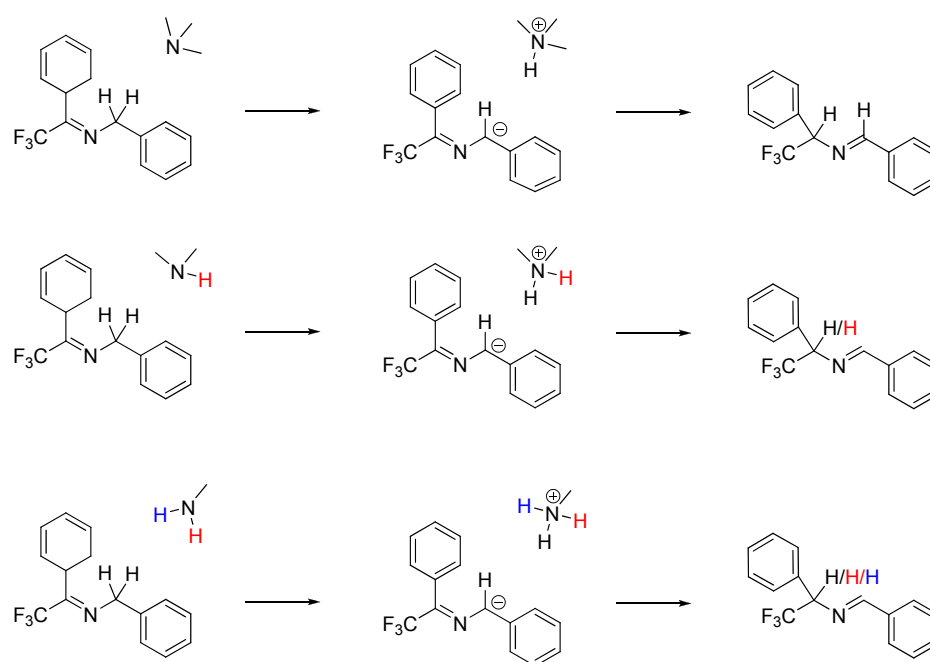
amine	deuterium incorporation in reaction of <b>30</b> (L=H)	hydrogen incorporation in reaction of <b>30</b> (L=D)
triethylamine	12.7%	28.5%
diethylamine	23.0%	42.1%
<i>t</i> -butylamine	39.4%	76.5%

Note: We used 5 mol% of the corresponding amine hydrochloride salt as a buffer in the reaction to eliminate the possibility of deprotonation by methoxide anion.

The results in Table 3 indicate that when **30** (L=D) is used, the preference to transfer the pulled-off deuterium back to the azaallylic anion is significantly diminished (compared to the preference in the corresponding protio case). Based on our observations, there is an H/D isotope effect of about 2. However, one factor complicates these experimental observations. It is rather difficult to quantify the amount of protons/deuterons that came from the solvent (methanol /  $d_4$ -methanol) that are incorporated in **31**. Studying this reaction in an aprotic solvent would simplify this problem as there will be no exchangeable protons in the solvent. Also, in order to interpret our experimental results and explore a possible role of dynamic effects in determining the product ratios, we were interested in studying this reaction computationally. It is difficult to computationally model all of the hydrogen bonding interactions present in a protic

solvent like methanol. Therefore we decided to conduct the same experiments in an aprotic solvent ( $d_6$ -benzene) and then compare the experimental results to easily calculable theoretical results in benzene.

### Scheme 5



Illustrated in Scheme 5 are the possible products that might be observed using the three different amines as base for the isomerization reaction in an aprotic solvent like benzene. It is obvious that under these conditions, in the absence of exchangeable protons in the solvent, the tertiary amine has no choice but to return the proton that it originally pulled off. By using **30** (L=H) and pre-deuterated 1° and 2° amines in benzene

we can determine the deuterium incorporation in the absence of the complicating solvent effects. Moreover, from the comparison of these results to the reaction of **30** (L=D) and protio amines in benzene we can estimate the H/D KIE. The results from the four experiments in benzene are presented in Table 4. It is interesting to note that though extent of the deuterium incorporation in benzene is lower as compared to methanol, (supporting the idea that methanol was indeed the source of some of the protons/deuterons seen in **31**) the isotope effect remains roughly the same. The reaction of **30** (L=H) with  $d_1$ - diethylamine should theoretically give 33% deuterium incorporation based on an H/D KIE of 2. Instead the deuterium incorporation is only 15.3%.

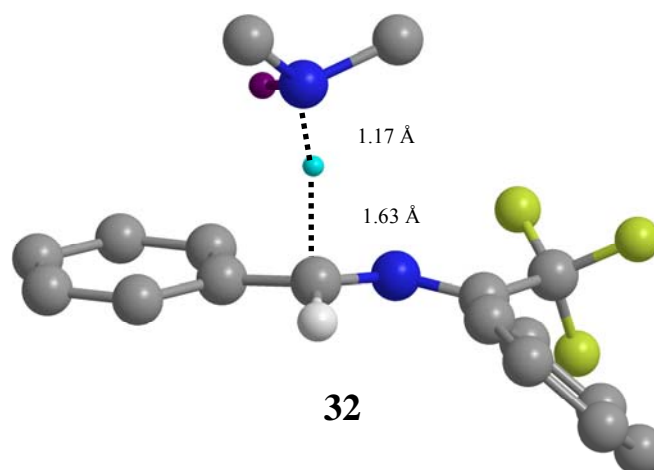
**Table 4.** Results from labeling studies in  $d_6$ -benzene

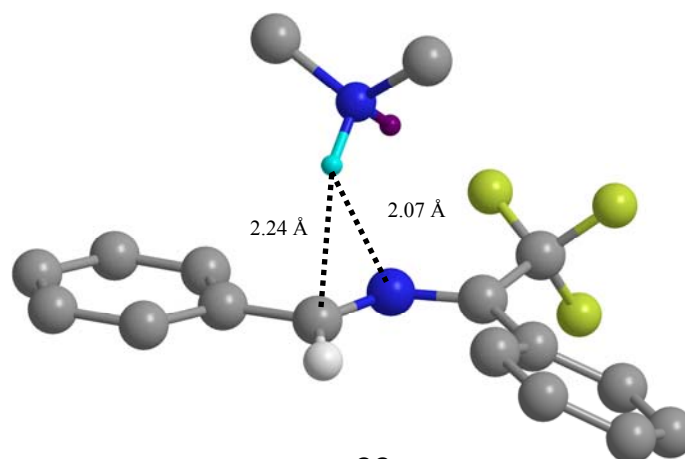
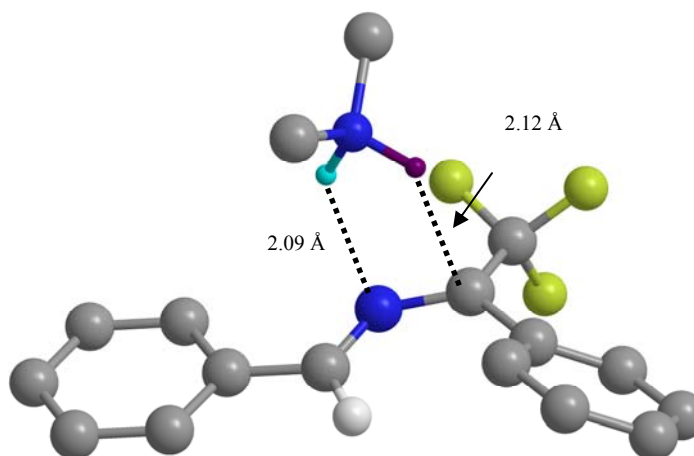
<b>Amine</b>	<b>deuterium incorporation in reaction of 30 (L=H)</b>	<b>hydrogen incorporation in reaction of 30 (L=D)</b>
$d_1$ - diethylamine	15.3%	32.4%
$d_2$ - <i>t</i> - butylamine	25.3%	47.5%

Having eliminated the possibility of exchange with solvent and having taking into account the contribution of the isotope effect to the product ratios, this result clearly indicate that there is a preference to return the proton that was originally pulled off from **30** to the final product **31**. With these results in hand, our next step was to theoretically model this reaction in benzene and attempt to understand our experimental observations and possibly explore the role of dynamic effects in determining the outcome of this reaction.

### 3.3 Theoretical and Dynamics Trajectory Calculations

The reaction of imine **30** (L=H) and dimethylamine was studied using B3LYP calculations employing a 6-31G\* basis set and an Onsager solvent model for benzene. Three distinct saddle points were located on the potential energy surface for this reaction. The first saddle point on the potential energy surface **32** represents the deprotonation of the **A** by dimethylamine. The next saddle point **33** corresponded to a 1,2 motion of the protonated amine with respect to original C=N bond. The minimum



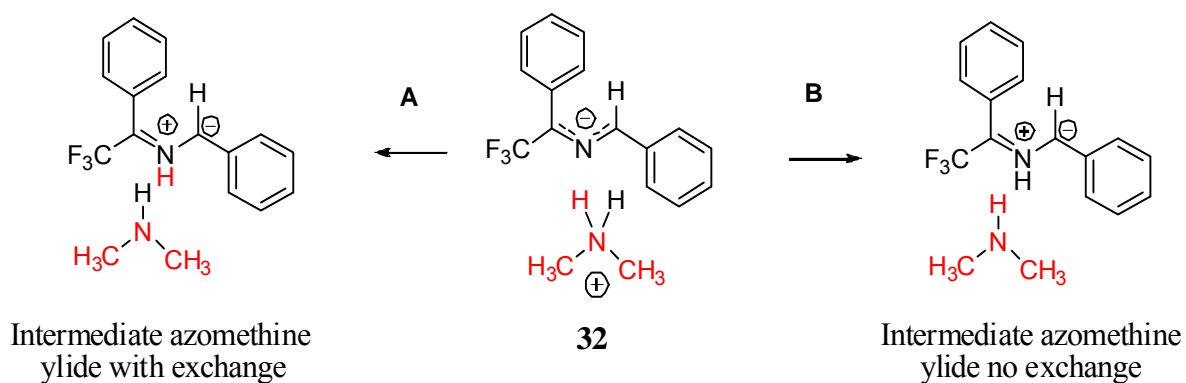
**33****34**

energy path from this second transition state leads to an intermediate azomethine ylide that was located as a minima on the potential energy surface. A saddle point **34** was located which represented a 1,2 motion similar to **32**, but on the product side i.e. with respect to the original N-C bond.

Transition structures **32** and **34** were starting points for the quasiclassical dynamics trajectories. With all atomic motions freely variable, the trajectories were initialized by giving each mode a random sign for its initial velocity, along with an initial energy

based on a random Boltzmann sampling of vibrational levels at 273.15 K, including zero-point energy. The mode associated with the imaginary frequency was treated as a translation and given a Boltzmann sampling of translational energy “forward” over the col. The starting atomic positions on the potential energy ridge in the area of the transition structures were randomized using a linear sampling of possible harmonic classical displacements for each normal mode, adjusting the kinetic energy for each mode accordingly. Employing a Verlet algorithm, 1-fs steps were taken until productive outcome was observed (intermediate, product or recrossing) up to a maximum of 500 femtoseconds. The results from 44 trajectories on both starting material and product side are shown below.

### Scheme 6

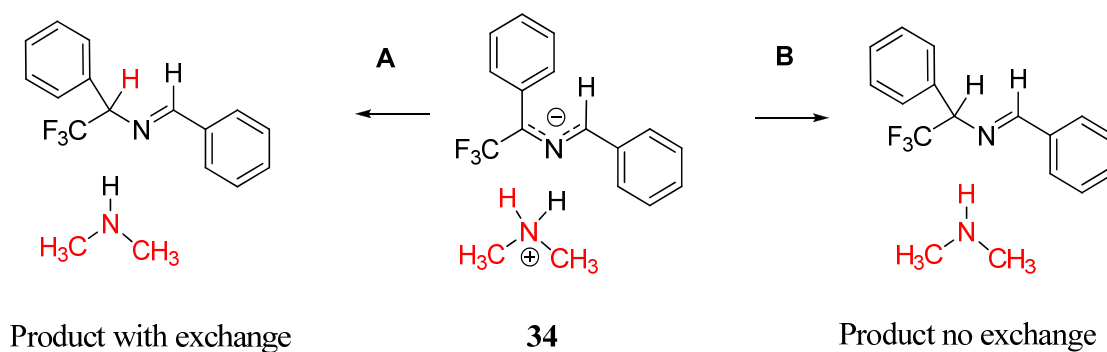


Total trajectories = 44; **A** trajectories = 30; **B** trajectories = 9; Recrossing trajectories=5.

Scheme 6 illustrates the results of the trajectories initiated from **32**. Two possible outcomes were deemed possible. The proton on the protonated amine shown in black is

the proton that was originally pulled off from the starting imine **30**. The red proton was originally on the dimethylamine. Outcome **A** represents those trajectories that go to the intermediate azomethine ylide by transferring the proton that was originally on the dimethylamine. Outcome **B** represents those trajectories that went to the same intermediate, but by putting back the same proton that was originally pulled off from **30**.

### Scheme 7



Total trajectories = 44; **A** trajectories = 35; **B** trajectories = 0; Recrossing trajectories = 9.

Trajectories initiated from **34** also had two possible outcomes (Scheme 7). The proton on the protonated amine shown in black is the proton that was pulled off from the intermediate azomethine ylide. The red proton was originally on the dimethylamine. Outcome **A** represents those trajectories that go to product by transferring the proton that was originally on the dimethylamine. Outcome **B** represents those trajectories that went to the same intermediate, but by putting back the same proton that was originally pulled off from intermediate azomethine ylide.

### 3.4 Discussion and Conclusion

Our experimental results cannot be reconciled by transition state theory. The product distribution is a result of the motion and momenta of atoms as they traverse the potential energy surface. The labeling studies provide indisputable evidence for a non-concerted proton transfer mechanism. The deuterium incorporation observed in the reaction catalyzed by triethylamine in  $d_4$ -methanol supports the idea that the contact ion pair is long lived and can exchange its protons with the solvent. The presence of exchangeable protons in the solvent complicates the mechanistic picture. The reactions in benzene simplify the mechanistic interpretation of the labeling experiments. The observation of 15% deuterium incorporation in the reaction of **30** (L=H) with  $d_1$ -diethylamine and 32% hydrogen incorporation in the reaction of **30** (L=D) with  $h_1$ -diethylamine suggests that the reaction has a propensity to transfer the hydrogen isotope that it originally pulled off **30**, the preference being more (by a factor of  $\sim 2$ ) when the isotope was a proton. Such an interpretation is simplistic and our theoretical calculations suggest that a more complex process is operational. A majority ( $\sim 75\%$ ) of the dynamic trajectory calculations initiated from the saddle point **32** go to an intermediate azomethine ylide *with exchange*. Starting from the saddle point on the product side, the trajectories almost exclusively go to product *with exchange*. Therefore the observed preference of **30** to isomerize most of the time by transferring the same proton is in fact a result of an exchange-exchange sequence as opposed to a single step process with no exchange occurring most of the time. Though there is no experimental evidence for the existence of this azomethine ylide intermediate, the remarkable agreement of experimental product ratios and those



derived from dynamic trajectory calculations of the secondary amine catalyzed reaction lend support to this proposed mechanism. This is yet another case where dynamic trajectory calculations can explain experimental observations, where conventional TST cannot even begin to make a crude prediction.

## CHAPTER IV

## DYNAMIC EFFECTS IN THE ROUGH ALLYLBORATION OF ALDEHYDES

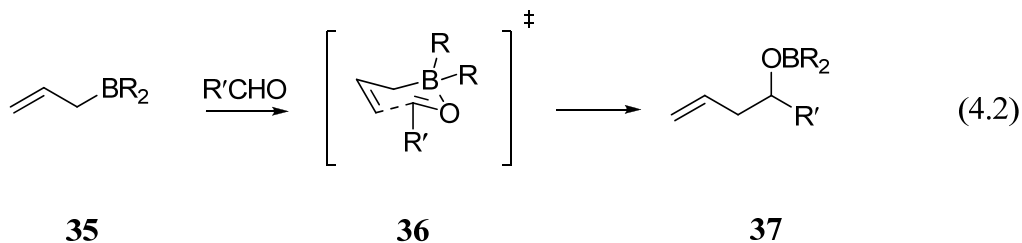
**4.1 Introduction**

A transition state is a hypersurface dividing starting materials from products for defining reactive trajectories. In conventional TST, this hypersurface is placed perpendicular to the minimum-energy path at a potential energy saddle point, and the reaction rate is associated with quasiequilibrium enthalpy and entropy of the transition state according to eq 4.1. It is well-recognized that this description is simplistic.<sup>9</sup> Indeed, the transmission coefficient  $\kappa$  that is incorporated into usual presentations of TST may be viewed as a correction for two complications that affect the rates of reactions, recrossing and tunneling.<sup>50</sup> Tunneling allows reactive trajectories that do not adhere to the classical limitation of the transition state energy, so that conventional TST underestimates the rate. To make up for this, a  $\kappa$  greater than unity may be incorporated as a correction. Recrossing occurs when trajectories pass through a transition state but pass back without affording product. Such trajectories are, in effect, counted in the free-energy of activation, lowering it, but they do not contribute to the rate. As a result, the rate is overestimated. A  $\kappa$  less than unity corrects for this. In variational transition state theory (VTST), the transition state hypersurface is itself repositioned to minimize the error engendered by recrossing. Outside of hydrogen-transfer and barrierless reactions, these complications are usually ignored with the assumption that their effect will be negligible. We describe here how recrossing and tunneling, along with an intriguing

$$k = \kappa \frac{kT}{h} e^{-\Delta G_{act}^0 / RT} = \kappa \frac{kT}{h} e^{-\Delta H_{act}^0 / RT} e^{\Delta S_{act}^0 / R} \quad (4.1)$$

interplay of the two, affect experimental observations in an ordinary and valuable organic reaction, the allylboration of aldehydes. The results particularly impact the mechanistic interpretation of KIEs.

The allylboration of aldehydes (eq 4.2) affords homoallylic alcohols and formally accomplishes an aldol reaction when coupled with oxidative cleavage of the alkene. Enantioselective versions of this reaction have proven particularly useful because the stereochemical and regiochemical outcome is readily predictable and is consistent with formal ene reaction proceeding by a chair-like transition state **2**.<sup>51</sup> Mechanistically, these are well-behaved reactions with straightforward bimolecular kinetics.<sup>52</sup> Gajewski observed a significantly inverse secondary deuterium KIE in the addition of the Roush allylboronate to benzaldehyde, consistent with rate-limiting addition to the carbonyl and inconsistent with rate-limiting single-electron transfer.<sup>53</sup> Theoretical studies have supported the basic mechanistic picture derived initially from experimental observations.<sup>54</sup>



We have recently observed that recrossing can play a substantial role in complex pericyclic reactions,<sup>20</sup> and exploratory trajectory calculations on simple allylboration

models suggested that recrossing could play a role in these reactions. We therefore undertook a detailed study of the important example of the Roush allylboration by a combination of experimental KIEs, conventional theoretical calculations, variational transition state theory, and trajectory calculations. These studies show how the underlying physics associated with experimental observations in these reactions are more complicated than usually considered.

## 4.2 Exploratory Theoretical Studies

To explore the role of recrossing in allylboration reactions, a series of transition structures for relatively simple model reactions were first located using B3LYP<sup>55</sup> and mPW1K<sup>56</sup> methods and a 6-31G\* basis set. (Full details of the structures located are included in the appendix.) These transition structures were then used as the starting point for quasiclassical direct dynamic trajectories on the respective potential energy surfaces, using Gaussian 03<sup>42</sup> to calculate forces at each point. With all atomic motions freely variable, the trajectories were initialized<sup>57</sup> by giving each mode a random sign for its initial velocity, along with an initial energy based on a random Boltzmann sampling of vibrational levels appropriate for 298.15 K, including zero-point energy. The mode associated with the imaginary frequency was treated as a translation and given a Boltzmann sampling of translational energy “forward” over the col. The starting atomic positions on the potential energy ridge in the area of the transition structures were randomized using a linear sampling of possible harmonic classical displacements for each normal mode, adjusting the kinetic energy for each mode accordingly. Employing a

Verlet algorithm, 1-fs steps were taken until either the allylboration products were formed (defined by a C-C distance  $< 1.55 \text{ \AA}$  and B-C distance  $> 2.2 \text{ \AA}$ ) or recrossing occurred to afford the starting materials (defined by a C-C distance  $> 2.4 \text{ \AA}$  and B-O distance  $> 1.85 \text{ \AA}$ ) up to a maximum of 500 fs. The results are shown in Table 5. A notable initial result was the observation of a high amount of recrossing in the reaction of formaldehyde with allyl boronate **38**. There was no significant difference on going from formaldehyde to acetaldehyde but the sterically demanding pivaldehyde surprisingly resulted in a decreased amount of recrossing trajectories (entries 2, 3). The overall amount of recrossing was lower on changing **38** to E and Z-crotyl boronates (**39**

**Table 5.** Results from quasiclassical trajectory studies (B3LYP/6-31G\*)

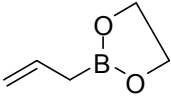
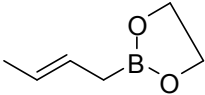
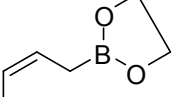
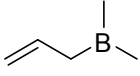
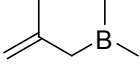
Entry	Allyl boron reagent	Aldehyde	Total trajectories	Recrossing trajectories
1	 <b>38</b>	HCHO	180	37 %
2		CH <sub>3</sub> CHO	100	35%
3		(CH <sub>3</sub> ) <sub>3</sub> CCHO	187	25%
4		PhCHO	132	21%
5		<i>p</i> -NO <sub>2</sub> PhCHO	63	32%
6		<i>p</i> -NH <sub>2</sub> PhCHO	94	12%

Table 5. cont'd,

Entry	Allyl boron reagent	Aldehyde	Total trajectories	Recrossing trajectories
7		<i>p</i> -OCH <sub>3</sub> PhCHO	89	17%
8	 <b>39</b>	CH <sub>3</sub> CHO	129	29%
9		(CH <sub>3</sub> ) <sub>3</sub> CCHO	59	22%
10	 <b>40</b>	CH <sub>3</sub> CHO	113	28%
11		(CH <sub>3</sub> ) <sub>3</sub> CCHO	65	23%
12	 <b>41</b>	CH <sub>3</sub> CHO	50	34%
13		CH <sub>3</sub> COCH <sub>3</sub>	21	14%
14	 <b>42</b>	CH <sub>3</sub> CHO	21	24%
15		CH <sub>3</sub> COCH <sub>3</sub>	76	29%

and **40**) and but the trend remained unchanged with pivaldehyde exhibiting lesser recrossing than acetaldehyde (entries 8-11). For the reaction of **38** and aromatic aldehydes a clear trend emerged where electron withdrawing para substituents showing an increase and electron donating para substituents a decrease in the amount of recrossing relative to benzaldehyde (entries 4-7). Changing from a boronate to the more Lewis-acidic dimethylboryl group had little effect on the observed recrossing (entries 12-15).

The most general trend in the data was that the amount of recrossing was dictated by the electrophilicity of the aldehyde component. This trend appeared to be correlated with the early versus late character of the transition state; more recrossing trajectories were observed from early transition states (more electrophilic aldehydes) as opposed to late transition states (less electrophilic aldehydes). For example, the incipient C-C bond distances at the transition state for formaldehyde and *p*-nitrobenzaldehyde (high recrossing) were 2.39 Å and 2.27 Å respectively, whereas those for *p*-anisaldehyde and *p*-aminobenzaldehyde (lower recrossing) were 2.15 Å and 2.13 Å respectively.

The recrossing observed in these systems was qualitatively different from the type of recrossing described in our earlier work with ketenes.<sup>20</sup> In the ketene case, recrossing occurred after fully forming a product bond. Here, the recrossing tended to occur relatively rapidly, after the trajectories had progressed only a short distance forward from the transition state. For example, for the recrossing trajectories in the reaction of **38** with *p*-nitrobenzaldehyde, the "forming" carbon-carbon bond reached on mean a minimum C-C distance of 2.07 Å, 0.2 Å past the distance at the transition structure

before going back to starting materials. Recrossing of this type may be viewed as resulting from an entropic tightening of the reaction channel along the reaction coordinate past the transition state. As a result, a portion of the trajectories hit the "walls" of the channel after crossing the transition state and bounce back to starting materials. Unlike the ketene case, the recrossing here should be largely statistically predictable. Due to various limitations of the calculational models, including the weakness of DFT methods in modeling dative bonds,<sup>58</sup> the particular amounts of recrossing observed in these trajectories is questionable. However, trajectory studies have performed notably well in predicting product ratios,<sup>5,12b,12c,15,20,59</sup> and our assumption was that the general trends observed here would parallel those present in reality. As will be discussed, experimental observations support this idea.

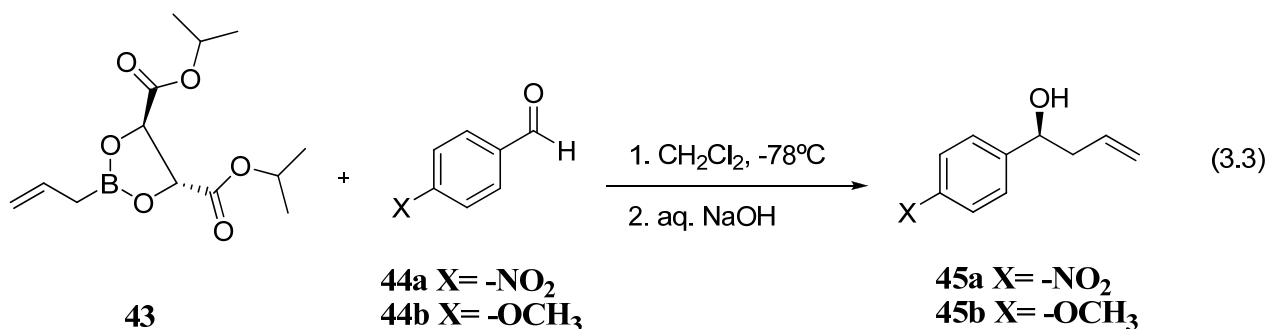
The role of recrossing in the exploratory trajectories also raised the intriguing idea that in an enantioselective allylboration, the enantioselectivity could be in part influenced by differing amounts of recrossing from two competing diastereomeric transition states. This led to the choice of the reactions of a Roush tartrate-modified allylboronate, **43**, with electronically differing aromatic aldehydes as the experimental system for study.

### 4.3 Experimental KIEs

The reactions of allylboronate **43** with *p*-nitrobenzaldehyde (**44a**) and *p*-anisaldehyde (**44b**) proceed smoothly at -78 °C and afford the homoallylic alcohols **45a** / **45b** in quantitative yield after basic hydrolysis. The <sup>13</sup>C KIEs for both components in



this reaction were determined from NMR analysis of the products at natural abundance.<sup>34,60</sup> Separate reactions were run to low conversion (~20%) in **43** (using



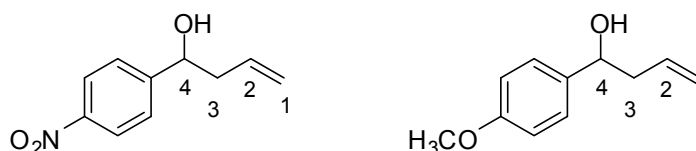
limiting aldehyde) and in aldehyde (using limiting **43**). The KIEs were then determined by comparison of the <sup>13</sup>C composition of the product **45** to product samples derived from reactions in which the same starting material was taken to 100% conversion.

The necessary comparison was conveniently accomplished by a comparative NMR analysis of the products obtained from the separate low-conversion reactions. This novel process eliminates the need for extra product isolation and analysis, and provides all of the <sup>13</sup>C KIEs for the reaction from the analysis of two product samples.

The <sup>13</sup>C KIEs from a series of independent experiments, as calculated from the changes in isotopic composition and the fractional conversion (see Chapter VI for full details) are presented in Table 6. The isotope effects in both cases can be qualitatively interpreted as rate limiting allylation of the aldehyde by the allyl boronate ester, with significant KIEs observed for all the carbons involved in bonding changes as in transition state **36**. However there is a striking difference in the KIEs observed for **44a**

and **44b**; The KIEs for the *p*-anisaldehyde reaction are larger, and the difference is particularly apparent at C1 and C4. It appeared notable that the KIEs were smaller in the

**Table 6.** Experimental intermolecular  $^{13}\text{C}$  KIEs ( $k_{12\text{C}}/k_{13\text{C}}$ ) for the reaction of tartrate modified allyl boronates and aromatic aldehydes. The three sets of KIEs for *p*-nitrobenzaldehyde and two sets for *p*-anisaldehyde represent independent experiments and the standard deviations of these measurements are indicated in parentheses.



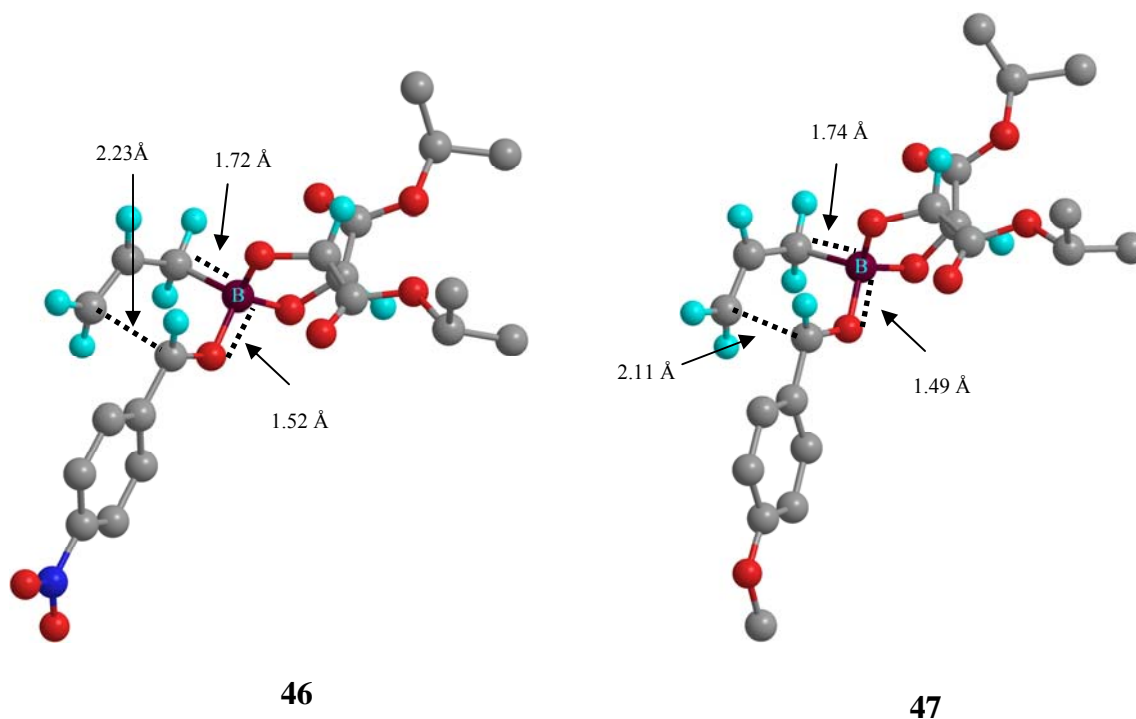
<i>p</i> -nitrobenzaldehyde	C1	C2	C3	C4
Expt 1	1.008(6)	0.997(4)	1.026(5)	1.032(6)
Expt 2	1.008(4)	0.997(4)	1.025(4)	1.031(7)
Expt 3	1.010(3)	0.999(3)	1.032(3)	1.035(4)
<i>p</i> -anisaldehyde				
Expt 1	1.019(8)	0.997(5)	1.036(5)	1.052(5)
Expt 2	1.023(5)	0.997(3)	1.034(3)	1.051(4)

system expected to undergo greater recrossing, but we defer a more detailed interpretation of the KIEs to after a consideration of the KIEs predicted by TST.

#### 4.4 Theoretical Structures and KIEs from TST

In order to interpret the experimental isotope effects, we computationally explored the reaction of **43** with *p*-nitrobenzaldehyde and *p*-anisaldehyde using DFT methods. Fully optimized geometries were obtained in both B3LYP and mPW1K calculations employing a 6-31+G\*\* basis set, either in the gas phase or using an Onsager<sup>36</sup> or PCM

solvent model<sup>37</sup> for dichloromethane. Lowest-energy transition structures **46** and **47** were located for the *p*-nitrobenzaldehyde and *p*-anisaldehyde reactions, respectively, from the PCM calculations. Both structures involve attack of the allyl moiety on the *si* face of the aldehyde; alternative structures for the *re* addition (not shown) were found to be higher in energy. Structures **46** and **47** are 9.7 kcal/mol and 12.2 kcal/mol respectively above the separate starting materials **43/44a (b)** (E + zpe), and in a free-energy estimate based on the unscaled harmonic frequencies, the composite  $\Delta G^\ddagger$  at standard state is **26.6 kcal/mol** and **29.3 kcal/mol** respectively.



The <sup>13</sup>C KIEs based on transition structures **46** and **47** were predicted from scaled theoretical vibrational frequencies<sup>39</sup> using conventional transition state theory by the Bigeleisen and Mayer method.<sup>7</sup> Tunneling corrections were applied using a one-

dimensional infinite parabolic barrier model.<sup>8</sup> The KIEs calculated based on these transition structures are shown in Table 7.

**Table 7.** Comparison of experimental KIEs for allylboration with KIEs predicted from conventional TST with a one-dimensional tunneling correction.

<i>p</i> -nitrobenzaldehyde	C1	C2	C3	C4
Expt 1	1.008(6)	0.997(4)	1.026(5)	1.032(6)
Expt 2	1.008(4)	0.997(4)	1.025(4)	1.031(7)
Expt 3	1.010(3)	0.999(3)	1.032(3)	1.035(4)
B3LYP/6-31+G**	1.017	0.998	1.035	1.040
B3LYP/6-31+G**(PCM)	1.016	0.998	1.036	1.043
MPW1K/6-31+G**	1.012	1.000	1.036	1.037
<i>p</i> -anisaldehyde				
Expt 1	1.019(8)	0.997(5)	1.036(5)	1.052(5)
Expt 2	1.023(5)	0.997(3)	1.034(3)	1.051(4)
B3LYP/6-31+G**	1.020	0.997	1.039	1.050
B3LYP/6-31+G**(PCM)	1.019	0.998	1.040	1.054
MPW1K/6-31+G**	1.015	0.999	1.039	1.050

The agreement between the predicted KIEs and those observed experimentally for the allylboration of *p*-anisaldehyde is striking. The normal interpretation of such agreement would be that the transition structure **47** (varying slightly in the differing calculations) is an accurate depiction of the transition state for the experimental reaction. However, the agreement of prediction with experiment for the *p*-nitrobenzaldehyde reaction is notably weaker. In particular, the observed KIEs for the *p*-nitrobenzaldehyde allylboration are much smaller at C1, C3 and C4 than those predicted from TST with the tunneling correction.

One might consider the possibility that disagreement between experiment and prediction for the *p*-nitrobenzaldehyde reaction is simply the result of inaccuracy in the calculated structures (and their frequencies from which the KIEs are calculated). Inaccuracy in the transition structures would not be surprising; as mentioned previously DFT calculations are known to be inaccurate with regard to dative bonds to boron.<sup>58</sup> However, such errors would not account for the difference between the accurate predictions in the *p*-anisaldehyde system versus the inaccurate predictions in the *p*-nitrobenzaldehyde system.

#### 4.5 Qualitative Effects of Recrossing

Since the error in the predicted KIEs comes in a system that would be expected to involve a relatively large amount of recrossing based on trajectories studies, it is of interest to consider the possible effects of recrossing on the isotope effects. Little is known in this regard, but one effect of recrossing may be expected on general principle.

Variational transition state theory corrects for statistically predictable recrossing by moving the transition state dividing surface away from the potential energy saddle point



**Figure 8.** Potential energy (black) and Free energy (blue) paths for the reaction of (a) *p*-nitrobenzaldehyde and (b) *p*-anisaldehyde

in such a way that the recrossing is minimized. For a canonical ensemble, recrossing is minimized when the variational transition state is placed at the free-energy saddle point. To the degree that recrossing is statistically predictable, it may be expected that greater recrossing in a system would correlate with a greater distance between the potential-energy saddle point and the free-energy saddle point.

The free energy saddle point for **44a** is significantly shifted from the potential energy saddle point (Figure 8a). For **44b** however, the two almost coincide (Figure 8b). Tunneling occurs through potential energy barriers and is represented by the horizontal red line in Figure 8. For **44a**, after having tunneled through the potential energy barrier, the reaction finds itself at the wrong side of the free energy barrier. Since the two barriers almost coincide for **44b**, tunneling takes the reaction through both barriers.

**Table 8.** Predicted KIES for allylboration of **44a/b** without tunneling.

<b><i>p</i>-nitrobenzaldehyde</b>	<b>C1</b>	<b>C2</b>	<b>C3</b>	<b>C4</b>
B3LYP/6-31+G**	1.017	0.997	1.029	1.035
B3LYP/6-31+G**(PCM)	1.016	0.997	1.029	1.037
MPW1K/6-31+G**	1.012	0.999	1.030	1.034
<b><i>p</i>-anisaldehyde</b>				
B3LYP/6-31+G**	1.019	0.997	1.028	1.042
B3LYP/6-31+G**(PCM)	1.018	0.996	1.026	1.043
MPW1K/6-31+G**	1.014	0.998	1.028	1.042

An experimental consequence of this observation is that tunneling would be decreased in the *p*-nitrobenzaldehyde system as compared to the *p*-anisaldehyde system. The predicted KIEs without including the tunneling correction are shown in Table 8. Careful analysis of the results presented in Table 7 and Table 8 leads to two key conclusions 1. experimental KIEs for **44a** are closer to the predicted KIEs without tunneling and for **44b** is closer to the KIEs with the tunneling correction. This observation is also in the right direction with regard to the trend in the observed recrossing in the dynamic trajectory simulations, since after ending up on the wrong side of the free energy barrier **44a** recrosses more than **44b**. 2. Heavy atom tunneling contributes significantly to the predicted isotope effects. However, the contributions from tunneling to the predicted isotope effect are not the same for **44a** and **44b**.

#### 4.6 Variational TST Predictions

Lastly, detailed VTST and tunneling analyses were carried out using POLYRATE<sup>41</sup> and Table 9 enlists the predicted KIEs calculated from comparing the reaction rates calculated for the parent system versus the rates calculated with <sup>13</sup>C labels at the respective carbons. The three sets of number listed in Table 9 (after the experimental KIEs) are the predicted KIES from TST, TST with zero curvature tunneling (TST-ZCT) and canonical variational transition state theory with small curvature tunneling (CVT-SCT). These results are in accord with the earlier predictions and lend support to the importance of a variational TST treatment and detailed tunneling calculations in the quantitative interpretation of KIEs in this reaction.

**Table 9.** KIE predictions using the rate calculation program POLYRATE

<b><i>p</i>-nitrobenzaldehyde</b>	<b>C1</b>	<b>C2</b>	<b>C3</b>	<b>C4</b>
Expt 1	1.008(6)	0.997(4)	1.026(5)	1.032(6)
Expt 2	1.008(4)	0.997(4)	1.025(4)	1.031(7)
Expt 3	1.010(3)	0.999(3)	1.032(3)	1.035(4)
B3LYP/6-31G* - TST	1.018	0.996	1.025	1.036
B3LYP/6-31G* - TST-ZCT	1.020	0.997	1.031	1.040
B3LYP/6-31G* - CVT-SCT	1.020	0.996	1.032	1.042
<b><i>p</i>-anisaldehyde</b>				
Expt 1	1.019(8)	0.997(5)	1.036(5)	1.052(5)
Expt 2	1.023(5)	0.997(3)	1.034(3)	1.051(4)
B3LYP/6-31G* - TST	1.024	0.997	1.023	1.042
B3LYP/6-31G* - TST-ZCT	1.026	0.998	1.034	1.049
B3LYP/6-31G* - CVT-SCT	1.027	0.998	1.036	1.052

#### 4.7 Discussion and Conclusions

The objective of this study was to observe the experimental effects of recrossing. The hypothesis was that experimental KIEs would deviate more strongly from predicted KIEs (based on TST) for systems with more recrossing (**44a**) than those with less recrossing (**44b**). Most of the statistical recrossing is predictable by VTST. This is true for the reaction of **44b** but the experimental KIEs for **44a** are markedly different from the VTST predictions. This indicates that extensive recrossing observed theoretically does contribute to the KIEs observed in this reaction. Large uncertainties in theoretical calculations, associated with the estimation of the contribution of recrossing to the KIEs, make an accurate quantitative prediction of KIEs for this reaction extremely difficult. In conclusion, our results point to importance of considering the effect of recrossing (that is not easily predicted by VTST) in interpreting the experimental KIEs for the Roush allylboration of **44a**.



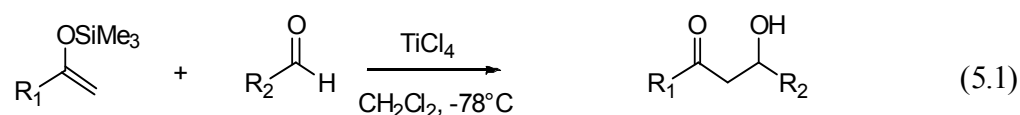
## CHAPTER V

## MECHANISM OF MUKAIYAMA ALDOL REACTION

**5.1 Directed Aldol Reactions**

Aldol reactions are powerful chemical transformations that form a carbon-carbon bond and potentially generate two new stereogenic centers. For over a hundred years, the synthetic utility of the crossed aldol reaction was severely limited by the formation of complex product mixtures containing a variety of cross and self condensation products. In the early 1970's, Mukaiyama and coworkers reported the reaction of silyl enol ethers with carbonyl compounds mediated by  $\text{TiCl}_4$  (eq 5.1).<sup>61,62</sup> This 'directed' aldol reaction was a major advance in the control of aldol reactions. Chemo- and regioselective aldol reactions could now be performed by using a suitable combination of a stable preformed enol derivative, a carbonyl compound, and a Lewis acid. Several Lewis acids have since been found to catalyze this transformation<sup>63</sup> and considerable work has been directed towards carrying out this transformation catalytically and/or enantioselectively.

The mechanism of this reaction is highly dependent on the reaction conditions and

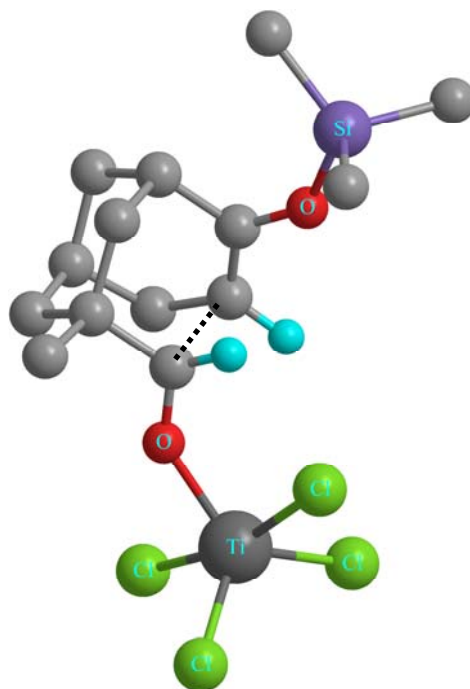
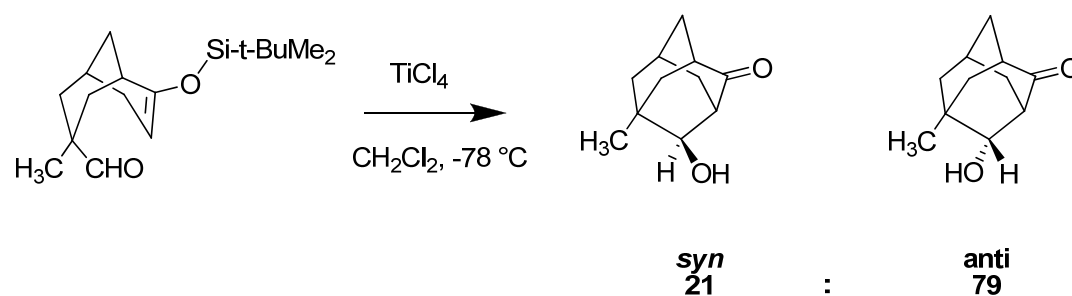


the nature of the Lewis acid used. It is therefore unlikely that all Mukaiyama aldol reactions occur by the same mechanism. Almost 40 years since the first report and despite its vast popularity, it is rather surprising to note that several key mechanistic aspects of the  $\text{TiCl}_4$  mediated aldol reaction remain unexplained. In the original publication, Mukaiyama proposed a mechanism that involved the formation of a trichlorotitanium enolate from the silyl enol ether (by elimination of trimethylsilyl chloride) that then reacts with the carbonyl compound.<sup>61</sup> However during the study of related reactions mediated by  $\text{TiCl}_4$ ,<sup>64,65</sup> it was found that the role of the Lewis acid ( $\text{TiCl}_4$ ) was to activate the carbonyl component towards the reaction with nucleophiles. Based on this finding, Mukaiyama revised the original mechanistic hypothesis to one that involves nucleophilic attack of the silyl enol ether on the carbonyl compound which is activated by coordination to the  $\text{TiCl}_4$ .<sup>62</sup>

The current mechanistic understanding of this reaction is based largely on stereochemical studies. In most cases, metal enolates are not believed to be involved in the reaction. The Zimmerman-Traxler transition state model,<sup>66</sup> which is usually invoked to explain the stereochemical outcome of aldol reactions of metal enolates, fails to account for stereochemical observations. The simple diastereoselectivity observed in the aldol product is found to be independent of the double bond geometry of the prochiral enol silane.<sup>67</sup> Over the years, mechanistic studies using a variety of substrates and Lewis acids have led to the proposal of contrasting stereochemical models for the mechanism of this reaction.<sup>68</sup> Barring certain exceptions, the stereochemical observations have been rationalized by considering acyclic (open) transition state models first put forward by

Heathcock and co-workers.<sup>69</sup> The current consensus on the mechanism of the Mukaiyama aldol reaction mediated by  $\text{TiCl}_4$  is based on a study of an intramolecular aldol reaction by Denmark and co-workers.<sup>70</sup> Based on the predominantly *anti* product observed, a preference for the open transition state with an anti-periplanar orientation of

**Scheme 8.**

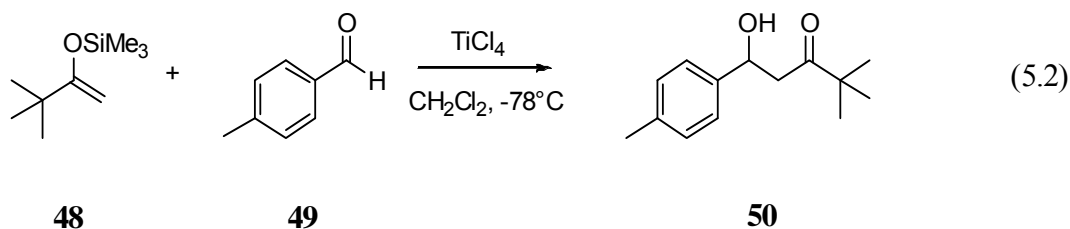


the double bonds is proposed to be key in determining the stereochemical outcome of this reaction as shown in Scheme 8. The applicability of this model to a more flexible intermolecular reaction is uncertain.

Experimental kinetic isotope effects (KIEs) and theoretical calculations are powerful probes that can shed light on the transition state geometry and rate-limiting step of a reaction. To the best of our knowledge, there have been no isotope effect studies for this reaction. Also, considering the importance of this reaction and the absence of a convincing mechanistic model, it is rather surprising that the Mukaiyama aldol reaction has received such little calculational scrutiny.<sup>71</sup> We decided to undertake a combined experimental and calculational study of the TiCl<sub>4</sub> mediated aldol reaction in order to distinguish between the various mechanistic models and to gain insight into the key features of this synthetically important reaction.

## 5.2 Experimental KIEs

The reaction of the trimethylsilyl (TMS) enol ether of pinacolone (**48**) and *p*-tolualdehyde (**49**) was chosen for the determination of <sup>13</sup>C and <sup>2</sup>H KIEs (eq 5.2).



Optimized reaction conditions for isotope effect studies involved addition of 1.1 equivalent  $\text{TiCl}_4$  to a mixture of **48** (1.1 equivalent) and **49** (1 equivalent) in  $\text{CH}_2\text{Cl}_2$  maintained at  $-78^\circ\text{C}$ .

The  $^{13}\text{C}$  and  $^2\text{H}$  KIEs for the aldehyde component in this reaction were determined at natural abundance by NMR methodology. Independent reactions were taken to  $65\pm 2\%$  and  $75\pm 2\%$  conversion in **49**, then the unreacted **49** was reisolated by an aqueous neutralizing workup and chromatography. The  $^{13}\text{C}$  and  $^2\text{H}$  composition of **49** was then analyzed by NMR compared to a sample of **49** that was not subject to the reaction conditions. In this analysis, the  $^{13}\text{C}$  and  $^2\text{H}$  peaks for the *p*-methyl group of **49** were used as a standard with the assumption that the isotopic composition in this position is unchanged. From the changes in isotopic composition in the other positions and the

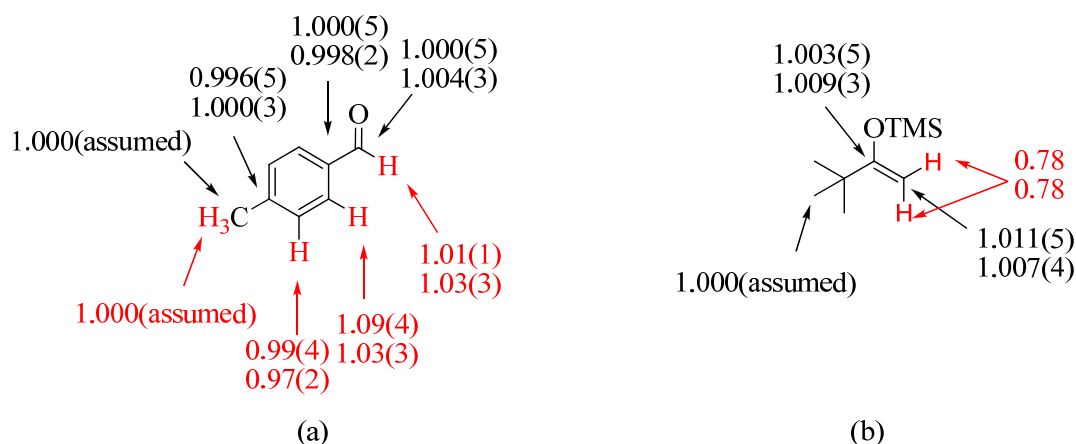


**Figure 9.** Experimental KIEs for (a) *p*-tolualdehyde and (b) pinacolone –  $^{13}\text{C}$  KIEs are in black and the  $^2\text{H}$  KIEs are in red. The two sets of KIEs represent two independent experiments and the standard deviations of these measurements ( $n = 6$ ) are indicated in parentheses.

reaction conversions, the  $^{13}\text{C}$  and  $^2\text{H}$  KIEs were calculated as described previously in Chapter I. The resulting KIEs are shown in Figure 7a.

The  $^{13}\text{C}$  KIEs for the silyl enol ether component were determined in an analogous way. Two separate reactions were taken to  $75\pm 2\%$  conversion in **48** by using limiting **49**. A complication in this process is that **48** hydrolyzes during work-up and could only be recovered as the corresponding ketone. To obtain a standard for the NMR measurements on the recovered pinacolone, unreacted **48** was converted quantitatively to pinacolone by an acidic hydrolysis. The  $^{13}\text{C}$  isotopic composition of the pinacolone recovered from the aldol reaction was then compared to that of the standard sample by  $^{13}\text{C}$  NMR, assuming that the isotopic composition in the methyl groups of the *t*-butyl group was unchanged. The  $^{13}\text{C}$  KIEs for **48** derived from this analysis are shown in Figure 7b.

Finally, the  $k_{\text{H}}/k_{\text{D}}$  for **48** was determined by analyzing the deuterium content in aldol product **50**, from reactions run using partially deuterated **48**, taken to partial conversion in **48**. The partially deuterated **48** contained  $\sim 69\%$  net deuterium in the two alkene protons. Analysis of the product **50** showed that the net deuterium content in the corresponding methylene position of **50** was about 73%. From the comparison of the net deuterium content and the fractional conversion, the  $k_{\text{H}}/k_{\text{D}}$  from two independent measurements was found to be 0.78.

Qualitatively, the complete set of KIEs in Figure 7 appear enigmatic at first glance. As a starting point for interpreting these KIEs, it should be recognized that the KIEs measured in competition reactions, as here, reflect the first irreversible step undergone

by a substrate. This is often the rate-limiting state for a reaction, but it need not be. It should also be recognized that the first irreversible step for two separate substrates in a bimolecular reaction need not be the same, though they often will be.

Within this context, the KIEs for **49** appear most unusual. The absence of a significant isotope effect for the carbonyl carbon of **49** seems to rule out carbon-carbon bond formation as the first irreversible step for the aldehyde. The slightly normal  $k_H/k_D$  for the aldehydic proton supports this conclusion. The H/D KIE also weighs against the first irreversible step for the aldehyde being any step after formation of the carbon-carbon bond, as a significantly inverse H/D KIE would be expected for such possibilities. In this way, the KIEs for **49** seem to rule out any step along the pathway of the conventional mechanism, except perhaps coordination of the aldehyde with the  $TiCl_4$ .

The significantly inverse  $k_H/k_D$  for the olefinic protons of **48** suggests that the terminal olefinic carbon is undergoing or has already undergone a change in hybridization in the first irreversible step for **48**. This would be consistent with carbon-carbon bond formation as the first irreversible step for **48**, or any step subsequent to carbon-carbon bond formation, but that would not fit with the isotope effects for **49**. The carbon KIEs for **48** are also relatively small and are of a magnitude not normally associated with primary carbon KIEs. The KIE for the terminal olefinic carbon of **49** is significant, but it does not fit well with a carbon-carbon bond forming step. Overall, the KIEs suggest that a more expansive consideration of the mechanism will be required.

Some issues complicate this qualitative interpretation of the KIEs. The aldehyde **49** is likely strongly complexed to the excess  $\text{TiCl}_4$  under the reaction conditions and this complex would be the formal "starting material" for the KIEs for **49**. The involvement of such unusual structures makes uncertain the application of the normal expectations for isotope effects. For potential mechanistic possibilities involving titanium enolates or electron transfer, careful consideration of the nature of the isotopically discriminative step will be required. The theoretical study of mechanistic possibilities will allow a more quantitative interpretation of this fascinating set of experimental KIEs.

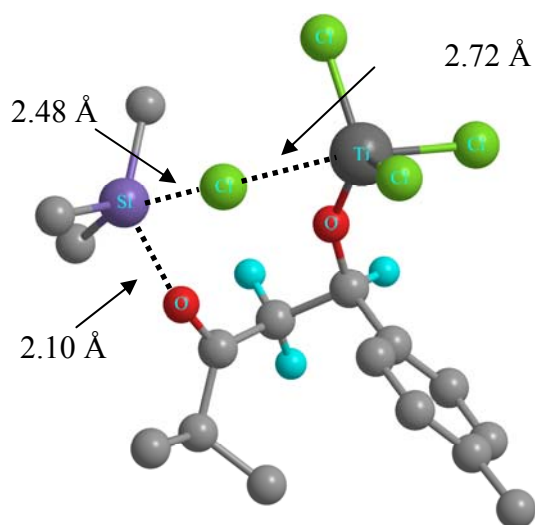
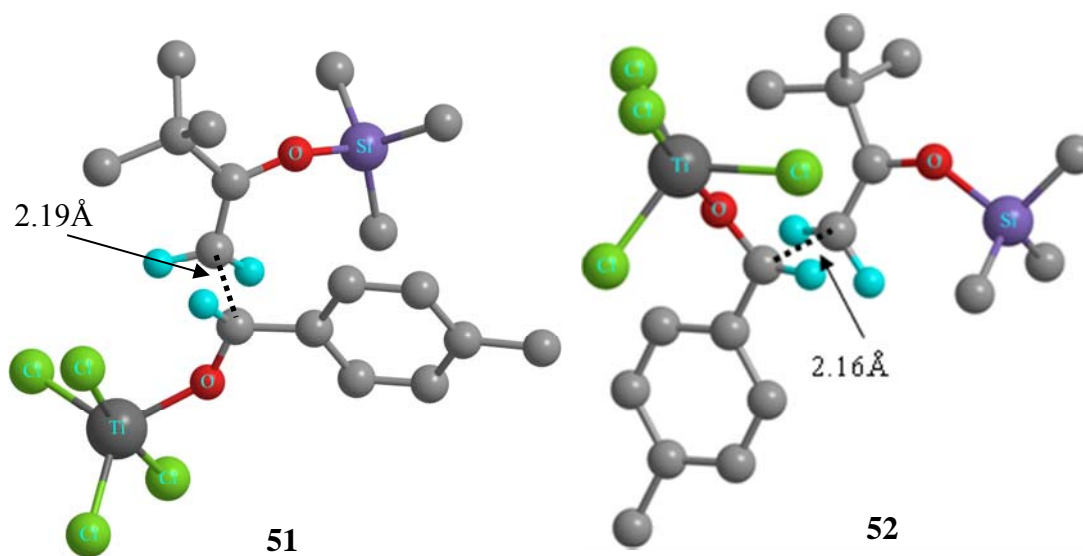
### 5.3 Theoretical Models

Exploratory calculations for the  $\text{TiCl}_4$  mediated aldol reaction of **48** with **49** were carried out in gas-phase B3LYP calculations employing a 6-31G\* or 6-31+G\*\* basis set. Important structures were then reoptimized using a PCM solvent model for dichloromethane and a 6-31+G\*\* basis set. In calculations where the titanium was intimately involved in the reaction mechanism, an SDD basis set<sup>72</sup> was employed for titanium. Radical structures associated with the electron transfer mechanism were calculated using unrestricted B3LYP/6-31G\*, and structures with potential diradical character were calculated using the guess=mix standard input in Gaussian03 to impart radical character to the calculated structures. As described below, a series of mechanistic possibilities were explored. The predicted KIEs based on these mechanistic models are presented in Section 5.4.



**Acyclic transition state (Heathcock/Denmark model)**

This standard mechanistic model for the  $\text{TiCl}_4$ -mediated Mukaiyama aldol reaction involves initial coordination of  $\text{TiCl}_4$  to the aldehyde followed by nucleophilic attack of the silyl enol ether to form the C-C bond. Though the experimental KIEs provided no



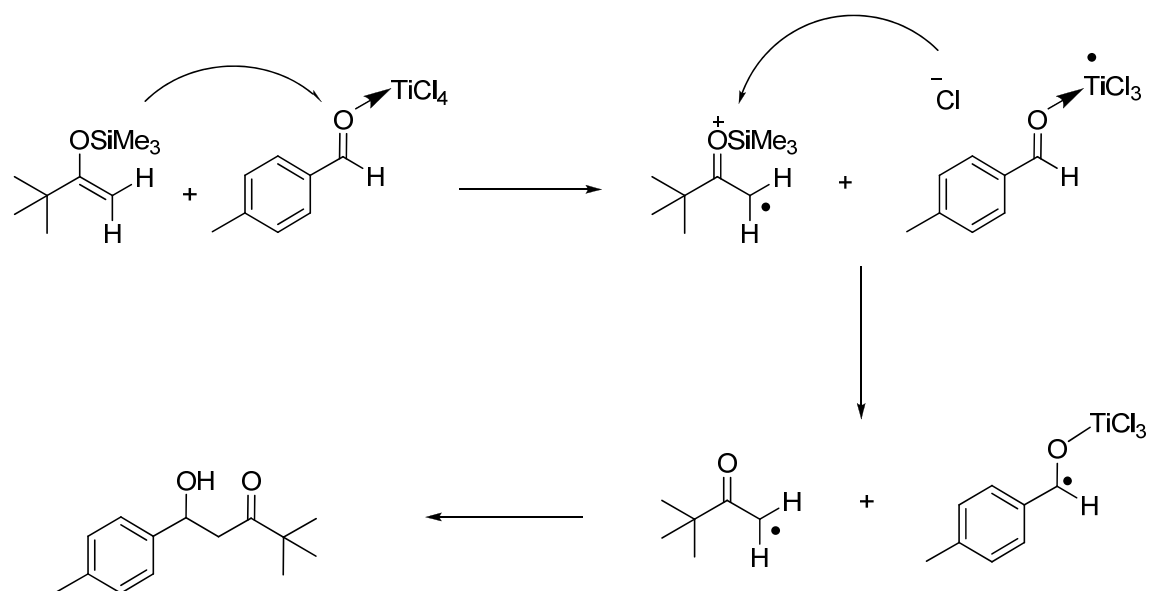
53

support for the C-C bond formation step to be rate limiting, we decided to model it using DFT calculations and theoretically predict KIEs. There is no energetic preference for the trans-antiperiplanar (**51**) v/s syn-clinal (**52**) approach of the nucleophile as it attacks the activated aldehyde. In fact, the syn-clinal orientation of double bonds is favored by 0.3 Kcal/mol (E+zpe B3LYP/6-31+G\*\* PCM solvent model for CH<sub>2</sub>Cl<sub>2</sub>). This initial attack is presumably followed by the displacement of the TiCl<sub>4</sub> by the TMS group or elimination of trimethylsilylchloride by a chloride, depending on whether the end product is the TMS protected aldol or the trichlorotitanium aldolate. We modeled the latter more probable possibility as transition state **53**. Upon aqueous workup, however, both of these pathways lead to the deprotected aldol product.

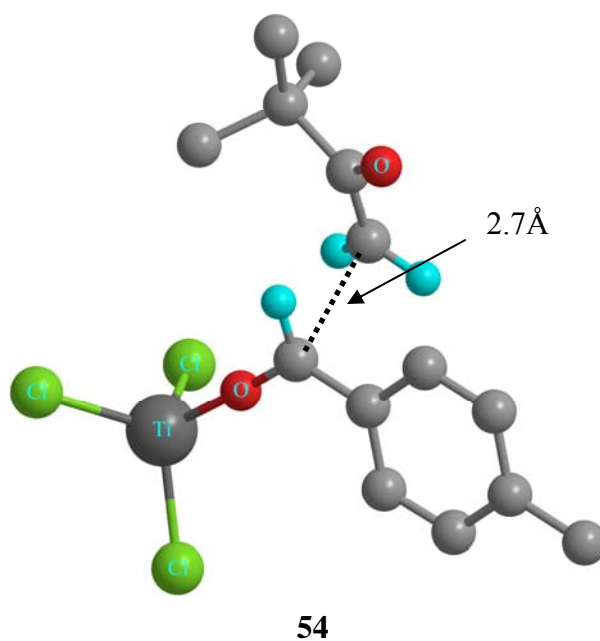
#### **Acyclic transition state (Radical coupling model)**

Another mechanistic possibility, shown in Scheme 9, is a radical-radical coupling mechanism initiated by an electron transfer.<sup>73</sup> The silyl enol ether is oxidized to a siloxonium radical while the TiCl<sub>4</sub>-complexed aldehyde is reduced to a TiCl<sub>4</sub> anion radical, which then undergoes fragmentation to ·TiCl<sub>3</sub> and Cl·. The ·TiCl<sub>3</sub> radical then adds to aldehyde to give a trichlorotitanium carbonyl radical. This radical subsequently couples with the pinacolone radical, generated by the elimination of TMSCl from the siloxonium radical by the attack of the Cl·, to give the final aldol product **50**.

Scheme 9



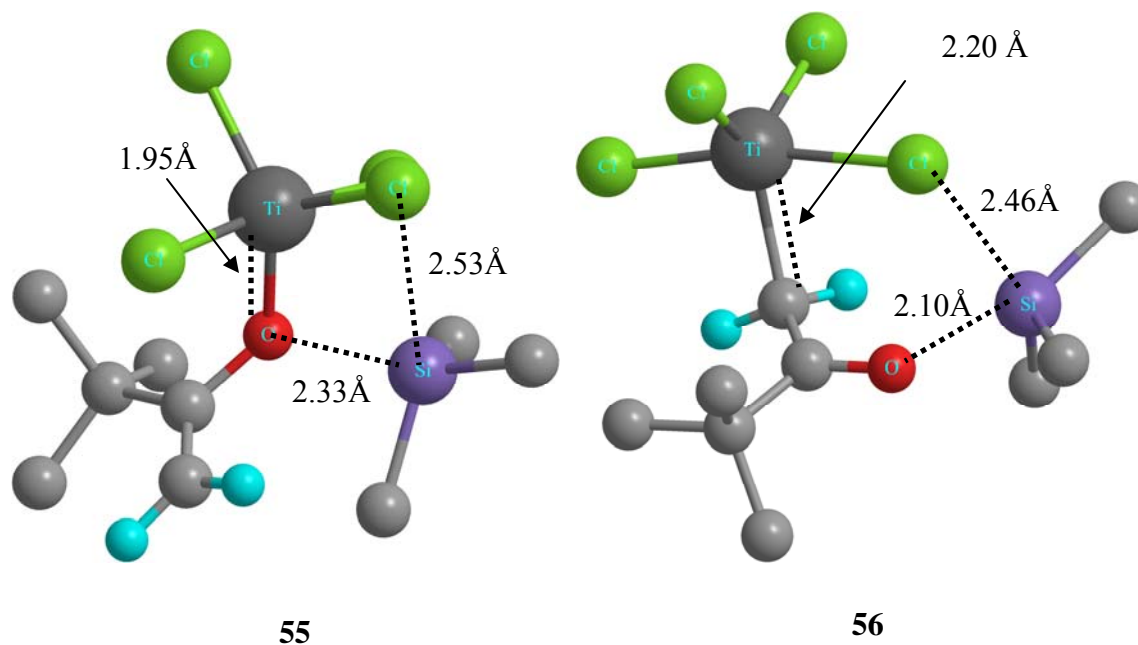
To explore this mechanism, the proposed intermediate radical structures, i.e., the radical cation of **48** and the radical anion of the  $\text{TiCl}_4$ -complexed **49**, were calculated using unrestricted B3LYP calculations and a PCM solvent model for DMSO. Equilibrium isotope effects (EIE) could be easily be determined versus optimized starting material structures. The C-C bond forming radical coupling step would be downhill and would face no potential energy barrier. However, there is a free energy barrier for the approach of two radical species. The variational transition state **54** for the radical coupling step was located by generating the free energy profile of the approach of the two radicaloid species in unrestricted B3LYP calculations with fixed distances.

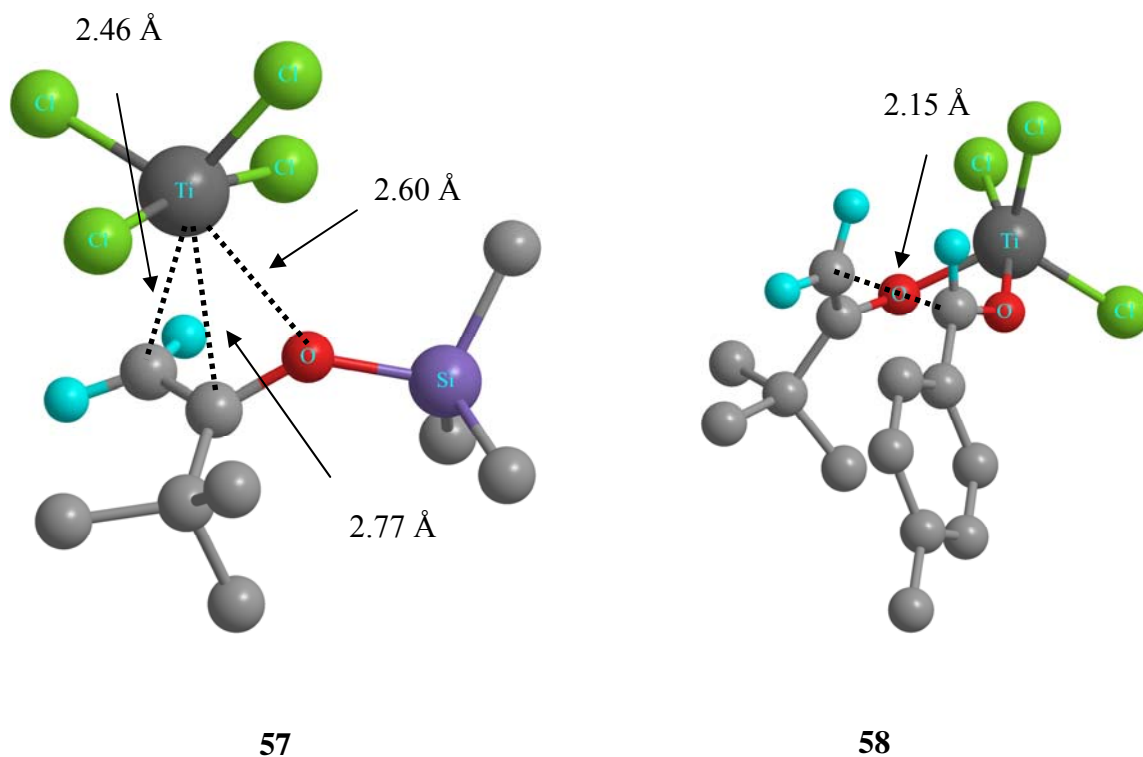


### Boat transition state (Kuwajima model)

A third mechanism that was explored was based on reactions of trichlorotitanium enolates, as reported by Kuwajima and co-workers.<sup>74</sup> In this mechanism, the reaction is initiated by the formation of a trichlorotitanium enolate from reaction of the silyl enol ether and  $\text{TiCl}_4$ . This could potentially occur in four ways – (a) direct attack of  $\text{TiCl}_4$  on the TMS bearing oxygen and eliminating  $\text{TMSCl}$  in a one-step process (transition structure **55**) (b) attack of  $\text{TiCl}_4$  on the terminal olefinic carbon and simultaneously eliminating  $\text{TMSCl}$  (transition structure **56**) followed by the migration of  $\text{TiCl}_3$  from the carbon to the oxygen (no transition structure located). (c) attack of  $\text{TiCl}_4$  on the terminal alkene carbon without concerted elimination of  $\text{TMSCl}$ , followed by migration of  $\text{TiCl}_4$  from carbon to oxygen (transition structure **57**) or (d) attack of  $\text{TiCl}_4$  on the TMS bearing oxygen without concerted elimination of  $\text{TMSCl}$  (no transition structure

located). In fully optimized B3LYP/6-31G\* calculations with SDD basis set on titanium and a PCM solvent model for  $\text{CH}_2\text{Cl}_2$ , transition structures **55** and **56** were found to be 35.1 and 38.9 Kcal/mol (E+zpe) above separate starting materials ( $\text{TiCl}_4$ /**48**). In free-energy estimates based on the unscaled harmonic frequencies, the composite  $\Delta G^\ddagger$ 's at a 1 atm standard state were predicted to be 48.8 and 51.7 kcal/mol. These barriers are too high to be energetically feasible. Transition structure **57** for the migration of  $\text{TiCl}_4$  from the terminal carbon to the oxygen is 19.8 (E+zpe) and 33.7 ( $\Delta G^\ddagger$ ) kcal/mol above  $\text{TiCl}_4$ /**48**. Once the trichlorotitanium enolate is formed by one of the above pathways, the coordination of the aldehyde to the titanium center and the subsequent reaction through a closed 6-membered boat transition state is predicted to be facile (transition structure **58**).





#### 5.4 Theoretical KIEs

The  $^{13}\text{C}$  and  $^2\text{H}$  KIEs based on transition structures **51-58** were predicted from scaled theoretical vibrational frequencies using conventional transition state theory by the Bigeleisen and Mayer method. Tunneling corrections were applied using a one-dimensional infinite parabolic barrier model. The table below presents the predicted KIEs corresponding to the three models discussed, in addition to calculated EIEs for the electron transfer steps. The experimental KIEs are also included for comparison. For all nucleophilic mechanisms, **49** and **48** were used for calculation of KIEs for aldehyde and silyl enol ether, respectively. For calculating KIEs for **49** in electron transfer mechanisms the **49-TiCl<sub>4</sub>** complex was used as starting material since the Lewis axis complexed aldehyde would be the kinetically relevant species in solution.

**Table 10.** KIE predictions for transition structures **51-58**. Highlighted in blue are the experimental KIEs (provided for comparison) and the predicted KIEs of theoretical models that best fit experiment.

	-CHO of <b>49</b>	=CH <sub>2</sub> of <b>48</b>	=C-O of <b>48</b>	$k_H/k_D$ -CHO of <b>49</b>	$k_H/k_D$ =CH <sub>2</sub> of <b>48</b>
<i>Expt 1</i>	<b>1.000(5)</b>	<b>1.011(5)</b>	<b>1.003(5)</b>	<b>1.01(1)</b>	<b>0.78</b>
<i>Expt 2</i>	<b>1.003(4)</b>	<b>1.007(4)</b>	<b>1.009(3)</b>	<b>1.03(3)</b>	<b>0.78</b>
<i>Mechanism 1 – TiCl<sub>4</sub> coordinated to 49, open anti-periplanar TS for attack of 48</i>					
<b>51</b>	1.061	1.040	1.000	0.63	0.61
EIE for formation of aldol-adduct from <b>51</b>	1.019	0.987	0.994	0.56	0.52
<b>53</b>	1.012	0.979	0.994	0.67	0.77
<i>Mechanism 2 – Initial electron transfer, C-C bond formation by radical coupling</i>					
EIE for initial electron transfer	<b>1.001</b>	1.023	1.000	<b>1.03</b>	1.37
<b>54</b>	1.055	1.061	1.006	0.79	1.32
<i>Mechanism 3 – formation of TiCl<sub>3</sub> enolate, C-C bond formation by 6-membered boat TS</i>					
<b>55</b>	NA	0.995	1.015	NA	0.971
<b>56</b>	NA	1.018	0.993	NA	0.90
<b>57</b>	NA	<b>1.012</b>	<b>1.009</b>	NA	<b>0.952</b>
EIE for formation of enolate-aldehyde complex	0.997	0.999	1.011	0.842	0.983
<b>58</b>	1.056	1.041	0.998	0.67	0.75

## 5.5 Discussion and Conclusion

From the results compiled in Table 10, it is clear no single model is consistent with all the experimentally determined KIEs. But there are a few key results worth noting. Regardless of the mechanism, experimental KIEs rule out the possibility of the rate-limiting carbon-carbon bond formation. None of the sets of predicted KIEs for the widely accepted Heathcock/Denmark mechanism are in accord with our experimental results. This weighs heavily against the possibility of this mechanism being operative. As mentioned in a previous discussion, KIEs reflect the first irreversible step that a

reactant undergoes during the course of a reaction. Therefore it is possible that **48** and **49** may have distinct steps being their first irreversible step.

The predicted equilibrium isotope effect (EIE) for the formation of radical anion complex of the aldehyde and  $\text{TiCl}_4$  in the electron transfer mechanism is strikingly similar to the experimentally measured KIEs. This suggests that the first irreversible step undergone by **49** is electron transfer. Indeed, the observation of carbon isotope effects near unity and slightly normal deuterium KIEs have been reported as diagnostics for rate limiting electron transfer.<sup>75</sup>

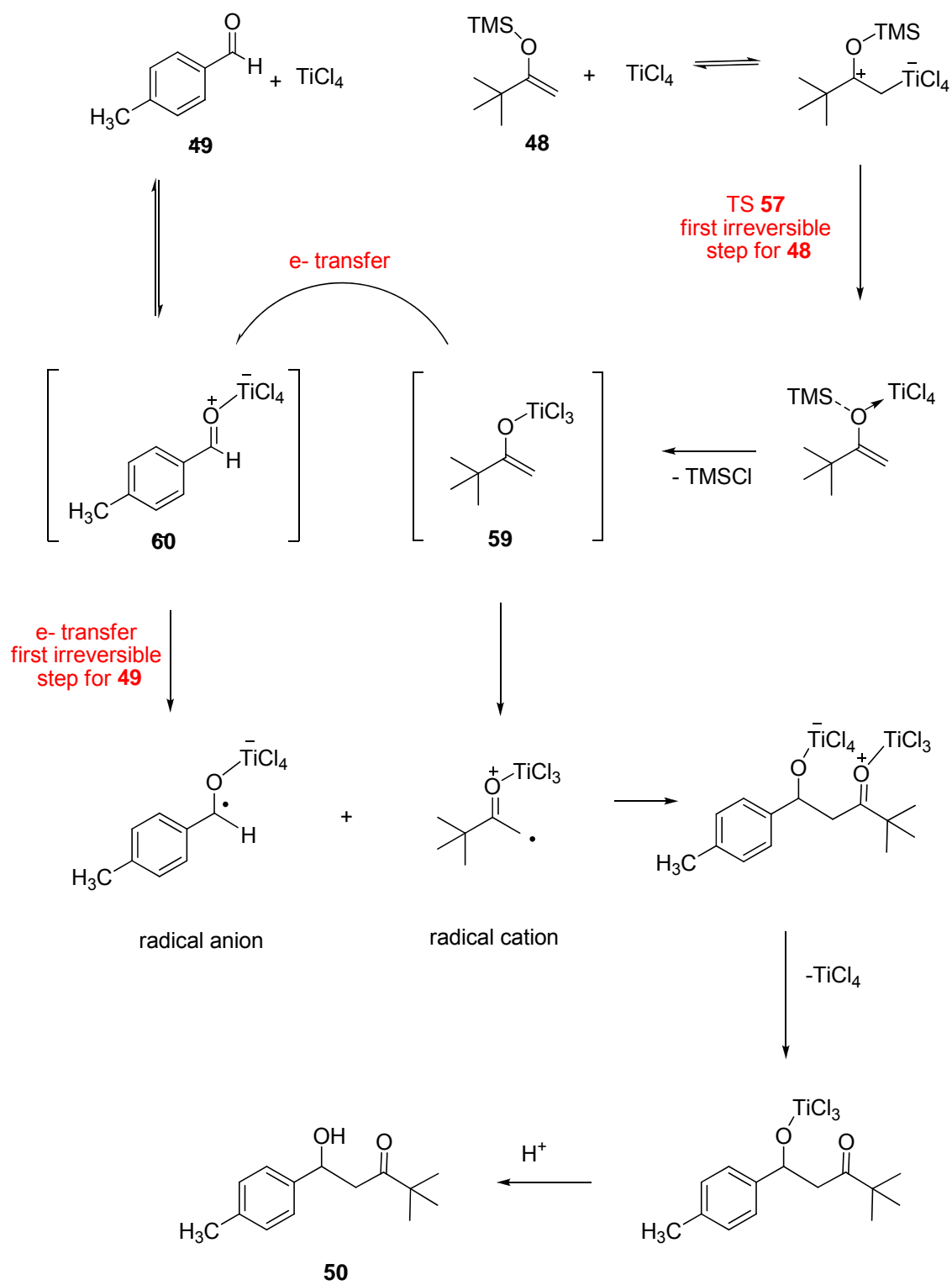
Electron transfer does not fit well as the first irreversible step undergone by **48**. The predicted EIE at the terminal olefinic carbon of **48** for the formation of the radical cation is significantly higher than the experimental isotope effect. Also, the predicted secondary deuterium EIE at this center is normal as opposed to the experimentally observed inverse KIE. It is therefore evident that electron transfer is not the first irreversible step for **48**. The predicted  $^{13}\text{C}$  and  $^2\text{H}$  KIEs for **48** based on transition state **57**, the migration of  $\text{TiCl}_4$  from terminal carbon to the oxygen of **48**, are in good agreement with the experimental KIEs for the silyl enol ether. Assuming that the coordination of  $\text{TiCl}_4$  to **48** is reversible, it is reasonable to expect that **57** might be the first irreversible step for **48**.

Based on the experimental isotope effects and theoretical studies, we propose a two- $\text{TiCl}_4$  model for the aldol reaction of **48** with **49** mediated by  $\text{TiCl}_4$ . Scheme 10 outlines this proposed mechanism. Both **48** and **49** reversibly coordinate to  $\text{TiCl}_4$  in the first step. After initial coordination to the terminal olefinic carbon of **48**, migration of  $\text{TiCl}_4$  from carbon to oxygen via transition state **57** would be the first irreversible step undergone by



**48.** The calculations suggest that this migration is energetically feasible and the predicted KIEs based on **57** are consistent with our experimental results. The intermediate species resulting from **57** eliminates TMSCl by either an inter or intramolecular mechanism to generate the trichlorotitanium enolate **59**. Electron transfer then occurs from **59** to the aldehyde-TiCl<sub>4</sub> complex **60** to generate a radical anion – radical cation pair. This step is the proposed rate-limiting step for the aldehyde – the experimental <sup>13</sup>C and <sup>2</sup>H KIEs are in excellent agreement with the predicted EIEs for the formation of the radical anion of **60**. Coupling of the radical ion pairs and regeneration of one equivalent of TiCl<sub>4</sub> would lead to the formation of the titanium aldolate, which after work up yields the aldol product **50**. A mechanism involving a titanium enolate has been largely excluded in discussing pertaining to the TiCl<sub>4</sub>-mediated aldol reactions primarily because reactions of trichlorotitanium enolates give predominantly *syn* products whereas TiCl<sub>4</sub>-mediated aldol reactions are generally *anti* selective.<sup>74,76</sup> Our proposal is consistent with this observation; a cyclic transition state that gives the *syn* product is sterically demanding and can be excluded in the two-TiCl<sub>4</sub> model.

## Scheme 10



While this mechanism is supported by the experimental KIEs for this particular experimental system, care must be exercised in extrapolating the mechanism to other Mukaiyama aldol reactions. As mentioned earlier, the mechanism of Lewis acid mediated aldol reactions is sensitive to the particular Lewis acid used. Some of our findings during the course of this study suggest that replacing the TMS enol ether by *tert*-butyldimethyl silyl enol ether (TBDMS) could alter the mechanism of the reaction. Further studies are underway to determine the scope of this electron transfer mechanism in Mukaiyama aldol reactions mediated by  $\text{TiCl}_4$ .

## CHAPTER VI

### EXPERIMENTAL PROCEDURES

#### 6.1 General Computational Procedures

Standard calculations of minima or transition structures employed Gaussian03. Default procedures in Gaussian03 were employed unless otherwise noted. Full structures and energetics are provided in the appendix. The program suite PROGDYN used for direct dynamics is listed at the end of the appendix as a series of component programs as either Unix shell scripts or awk or c programs. Gaussian03 was used to calculate the forces at each point in the trajectories. Some minor variations in PROGDYN were used to accomplish the special calculational experiments in which trajectories were initialized with extra energy along a vector aimed at the transition state. The program modifications used to accomplish these ‘cannonball’ trajectories are given at the end of the PROGDYN listings. Steepest-descent paths in mass-weighted coordinates were carried out in either of two ways: using the IRC option in Gaussian03 or using standard options available in PROGDYN. The latter uses a Euler algorithm with an adaptive step size and automatically decreasing step sizes when instability is detected. The standard Gaussian03 algorithm is tremendously faster while the PROGDYN algorithm succeeds in some cases where the more sophisticated Gaussian03 algorithm fails.

## GAUSSRATE (POLYRATE) input files and description of terms

Sample input files are included and are in **bold**. Calculation of pre-reactive complex, transition structure, and product complex (**p1.dat**, **p2.dat**, **p3.dat**) were performed in a manner similar to sample input files in the GAUSSRATE manual<sup>77</sup> and description of the keywords involved can be found therein. The description of keywords in the PATH section of the POLYRATE input file for calculation of dynamical rate constants (**p4.dat**) is shown in *regular italics* alongside the term. The output from these files served as input for the **p4.dat** file. The relevant output files from these calculations, used for determination of KIEs, are given in Section C of the Appendix. These calculations were used for KIE determination for the systems in Chapters II and IV. The examples shown in this section are from Chapter II.

**p1.dat** – *POLYRATE input file for calculation of pre-reactive complex*

**\*General** - *\* indicates section name*

**TITLE**  
**proline mediated aldol reactin**  
**calculation of pre-reactive complex**  
**END**

**ATOMS**  
**1 C**  
**2 C**  
**3 O**  
**.. ..**  
**.. ..**  
**31 H**  
**END**

**NOSUPERMOL** -

**\*OPTIMIZATION**

OPTMIN OHOOK  
OPTTS OHOOK

**\*SECOND**

HESSCAL HHOOK

**\*REACT1**

INITGEO HOOKS

GEOM

1

2

..

..

31

END

SPECIES NONLINRP

**# end of react1 section**

**p1.70** – *is the GAUSSRATE input file*

**\*GRGENERAL**

NOGRRESTART

**\*GRCOMMON**

**GRENER**

**#p B3LYP/6-31G\* UNITS=AU FCHK NOSYMM**

**scrf=(dipole,solvent=dms0,a0=5.15)**

**END**

**GRFIRST**

**#p B3LYP/6-31G\* FORCE UNITS=AU FCHK NOSYMM**

**scrf=(dipole,solvent=dms0,a0=5.15)**

**END**

**GRSEC**

**#p B3LYP/6-31G\* FREQ=NORAMAN UNITS=AU FCHK NOSYMM**

```

    scrf=(dipole,solvent=dms0,a0=5.15)
END

```

**GRLINK0** – *this section is to define the memory and number of processors*

```

    %nproc=4
    %mem=40mw
END

```

**p1.71** – *is the Gaussian input file for the calculation of complex.*

```

%nproc=4
%mem=40000000
#p B3LYP/6-31G* OPT FCHK scrf=(dipole,solvent=dms0,a0=5.15)

```

**proline pre-reactive complex**

```

0 1
C -0.952128 -3.825754 1.079237
C -1.018291 -2.622137 0.185451
.. .....
.. .....
H -1.711650 -4.555363 0.768196

```

The POLYRATE input files **p2.dat** and **p3.dat** and the GAUSSRATE input files **p2.70** and **p3.70** are for the calculation of product complex and transition state complex. The Gaussian input files **p2.73** and **p3.75** are for product complex and transition state complex, respectively, and are similar to **p1.71**.

**p4.dat** (only PATH and RATE sections, all others same as other .dat files)

**\*PATH**

**SCALEMASS 1.00** – *mass scale coordinates scale factor*

**RODS ON** – *re-orient the dividing surface*

**INTMU 3**

**SSTEP 0.001** – *step size for rate calculation*

**INH 10** – *frequency calculations performed after 10 steps along path*

**SRANGE** - range of  $s$  along the MEP

**SLP 1.00**

**SLM -1.00**

**END**

**RPM pagem** - method used to follow reaction path in this case Page-McIver

**SIGN REACTANT** - direction of unbound vector at saddle point

**IDIRECT 1** - initial direction of saddle point

**COORD CART** - The coordinate system

**FREQSCALE 0.9614** - frequency scale factor

**PRPATH** - print reaction-path information

**COORD 3 4** - determines what coordinates to follow along the reaction path

**INTERVAL 1** - determines how often to follow the specified coordinate

**XMOL** - makes it possible to visualize geometry changes along path in

**MOLDEN**

**END**

**EXFIRST** - performs extrapolation

**EXPROD** - direction of extrapolation

**EXNSTEP 200** - number of steps to be taken in extrapolation region

**EXSTEP 0.005** - mass-scaled step size

**END**

**EXSECOND**

**EXREACT**

**EXNSTEP 200**

**EXSTEP 0.005**

**END**

**SPECSTOP** - specify the range over which the MEP is to be computed

**CURVE vag**

**POINT savegrid**

**PERCENTDOWN 95.**

**END**

**\*TUNNEL**



**QUAD** – to specify the Gauss-Legendre quadrature points in each segment used in computing the Boltzmann average (NQE) and theta integrals (NQTH) in the tunneling calculations.

**NQE 40**  
**NQTH 40**  
**END**

**SCT** – performs small curvature tunneling calculation

**\*RATE**

**FORWARDK** – forward rate constants only

**SIGMAF 1** - sym. factor for forward reaction  
**CVT** – performs variational TST calculations

**TEMP** – desired temperatures for dynamical rate calculations

**200.**  
**298.15**  
**300.**  
**350**  
**400.**  
**500.**  
**600.**  
**800.**  
**1000.**  
**1500.**  
**2000.**  
**2400.**  
**END**

## 6.2 Experimental Procedures for ‘Corner Cutting in Organocatalysis’

### L-Proline catalyzed aldol reaction of **10** and acetone

To a well stirred solution containing 0.57 g (5 mmol) of L-proline in 250 mL of 8:2 DMSO/acetone was added 3.77 g (25 mmol) of **10**. After 30 min the reaction was quenched with 250 mL of saturated ammonium chloride and extracted 3 times into 250-

mL portions of diethyl ether. The organic layer was then washed with 250 mL of water to remove DMSO. The resulting organic layer was dried over anhydrous sodium sulfate and concentrated under reduced pressure. The crude mixture was purified by column chromatography using 3:1 mixture of hexanes/ethyl acetate as eluent. The fractions containing only the aldol product **11** were combined and 0.490 g of pure **11** was isolated.

### **L-Proline catalyzed aldol reaction of **12** and acetone**

For all 100% conversion reactions of **12**, 5.64 g (40 mmol) of **12** was added to a well stirred solution containing 0.92 g (8 mmol) of L-proline in 400 mL of 8:2 DMSO/acetone. After 90 min, when NMR analysis of a quenched aliquot showed complete consumption of **12**, the reaction was quenched with 400 mL of saturated ammonium chloride and extracted three times with 400-mL portions of diethyl ether. The organic layer was then washed with 400 mL of water to remove DMSO. The resulting organic layer was dried over anhydrous sodium sulfate and concentrated under reduced pressure. The crude mixture was purified by column chromatography using 9:1 mixture of hexanes/ethyl acetate as eluent. The fractions containing only the aldol product **13** were combined and 2.5 g of pure **13** was isolated. The low conversion reactions were run on the same scale but using only 0.23 g (2 mmol) of L-proline and were stopped within 10 min of addition of **12** to the reaction mixture. By this procedure three identical reactions were taken to 11%, 20% and 26 % conversion based on  $^1\text{H}$  NMR analysis, comparing the aromatic protons in starting-materials and product. The

aldol product **13** was isolated by flash chromatography using 1:9 mixture of ethyl acetate/hexane as eluent.

### **Dehydration of 13 using *p*-TsOH**

To a solution containing 2.1 g (10.5 mmol) of **13** in 20 mL of toluene was added 0.052 g (0.3 mmol) *p*-TsOH. The resulting mixture was allowed to reflux for 4 h with aliquots drawn at every hour to check for the complete disappearance of **13** by  $^1\text{H}$  NMR. Once complete, the reaction was quenched using 10 mL of 5% aqueous sodium bicarbonate. The organic layer was then washed successively with two 10-mL portions of water, dried over anhydrous sodium sulfate and concentrated under reduced pressure to afford a crude product mixture containing 1.8 g of **14** along with some trace **12** (< 2%). This product mixture was purified by flash chromatography using dichloromethane as eluent to afford 1.1 g of **14**. Six reactions (two each for each of the sets of KIEs determined) were run under identical conditions but different scales, depending on the amount of **13** isolated from the aldol reaction, to afford clean samples of **14** for NMR analysis.

### **Synthesis of soluble proline derivative 15 for kinetics studies**

To a mixture of 1.31 g (10 mmol) of trans-4-hydroxy L-proline and 10 mL (154 mmol) of anhydrous methanesulfonic acid, maintained at 0 °C, was added 2.26 g (14 mmol) of octanoyl chloride over a period of 10 min. The resulting mixture was allowed to warm up to room temperature and stirred overnight (20 h). The mixture was diluted

with 20 mL of diethyl ether and then neutralized with ammonium hydroxide. The organic layer was separated and concentrated under reduced pressure to afford a product mixture containing the proline derivative **15** and ammonium salt of methanesulfonic acid. This mixture was then washed twice with 20 mL of water to remove the salt. The crude product obtained was then recrystallized from a minimum volume of methanol to afford 1.53 g of white crystals of **15**.

### **Aldol reaction of **10** and acetone catalyzed by **15****

Side-by-side mixtures of 26.0 mg (0.1 mmol) of **15** in 10 mL of either 8:2 DMSO/acetone or 8:2 DMSO/*d*-6 acetone were equilibrated for 30 min at 25 °C, and the reactions were each initiated by the addition of 0.151 g (1 mmol) of **10**. Aliquots of  $\approx 0.5$  mL were drawn from each reaction at eight time points within the first 20 minutes of the reaction, quenched with  $\approx 0.5$  mL of saturated ammonium chloride, and extracted with 2 mL of diethyl ether. The organic layer was then concentrated under reduced pressure and the residue was analyzed by  $^1\text{H}$  NMR in  $\text{CDCl}_3$  to determine conversions. The  $k_{\text{H}}/k_{\text{D}}$  based on the *initial rate* was obtained from this data.

### **NMR measurements**

#### ***Intermolecular product KIE measurement***

NMR samples for each independent set (constitutes one low conversion and one 100% conversion sample) were prepared using 220, 475 and 490 mg of **14** in 5 mm NMR tubes filled to a constant height of 5 cm with  $\text{CDCl}_3$ . The  $^{13}\text{C}$  spectra were

recorded at 125.81 MHz using inverse gated decoupling, delay of 49 s (5 times T1) between calibrated  $\pi/2$  pulses, and a 7 s acquisition time to collect 511184 points. These parameters were used for two out of the three sets of experiments. Based on a slight change in T1, delays and acquisition times were adjusted for the third set. Integrations were numerically determined using a constant integration region for each peak. A zero-order baseline correction was generally applied, but no first-order correction was applied. Six spectra were recorded for each of the low conversion and 100% conversion samples.

#### *Intramolecular product KIE measurement*

By the procedure outlined earlier, two identical reactions of **10** were taken to 80.5% and 80% conversion of **10**. The product **11** was isolated and analyzed by  $^{13}\text{C}$  NMR using  $\text{CD}_3\text{OD}$  as solvent. Two separate NMR samples were prepared using 430 mg each of **11** in 5 mm NMR tubes filled to a constant height of 5 cm with  $d_4$ -methanol. The  $^{13}\text{C}$  spectra, centred between the methyl and methylene peak of **11**, were recorded at 100.482 MHz using inverse gated decoupling, delay of 34 s (8 times T1) between calibrated  $\pi/2$  pulses, and a 6.5 s acquisition time to collect 495946 points. Six spectra were recorded for each of the samples. Integrations were numerically determined using a constant integration region for each peak.

### 6.3 Experimental Procedures for ‘Base Catalyzed Isomerization of Fluorinated Imines’

#### Reaction in $d_4$ methanol

All deuterium incorporation experiments were carried out using 0.0263 g (0.10 mmol) of protio starting imine **30** (L=H) in 0.6 mL of  $d_4$ -methanol (~0.123 M) in a 5 mm NMR tube. Two equivalents of the appropriate amine (1°, 2° or 3°) were added to the reaction. The  $d_4$ -methanol was in sufficient excess to deuterate all of the amine. In order to carry out the reaction under buffered conditions, 5 mol % of the corresponding amine hydrochloride salt was added to the tube. The reaction was allowed to run at room temperature for approximately 24 h, the methanol and amine removed under reduced pressure, and the crude reaction mixture analyzed by  $^1\text{H}$  NMR in  $d_6$  benzene (since a small impurity showed up on the  $^1\text{H}$  NMR close to the shift for the transferred proton). All hydrogen incorporation experiments were carried out in exactly the same fashion except that 0.0265 g (0.10 mmol) of deuterated starting imine **30** (L=D) and protio methanol was used. A third reaction, which served as the standard reaction for  $^1\text{H}$  NMR integrations, was run according to the same procedure using protio starting imine **30** (L=H) and protio methanol.

#### Reaction in $d_6$ benzene

All experiments were carried out in exactly the same fashion as  $d_4$  methanol except for the following changes – (a) only 1° and 2° amines were used. (b) deuterium incorporation experiments were performed using pre-deuterated amines (c) both

deuterium and hydrogen incorporation experiments were carried out in  $d_6$ -benzene and NMR analysis was done without removing the amine and (d) no buffer was used.

### Synthesis of **30** (L=H)

A mixture of 1.07 g (10 mmol) of benzylamine, 2.61 g (15 mmol) of 2,2,2-trifluoroacetophenone, and 0.09 g of *p*-TsOH was refluxed in 30 mL of toluene for a period 2 days. Toluene was removed under reduced pressure and the residual mixture was loaded on a silica gel column. The column was eluted using a 98:2 mixture of hexanes/ethyl acetate and 1.58 g of **30** (L=H) was recovered.

### Synthesis of **30** (L=D)

An identical procedure was used for the synthesis of **30** (L=D) but using  $d_2$ -benzylamine with longer reaction times (3 days). Synthesis of  $d_2$ -benzylamine was accomplished by refluxing 1.03 g (10 mmol) of benzonitrile and 0.48 g (11 mmol) in 20 mL of diethylether. The resulting product mixture was worked up adding 0.5 mL of 15% sodium hydroxide and 1.5 mL of water. This mixture was filtered and extracted into diethylether and the  $d_2$ -benzylamine was obtained by removing the solvent under reduced pressure. The extent of deuterium incorporation observed in **30** (L=D) synthesized from  $d_2$ -benzylamine was greater than 99%, as confirmed by  $^1\text{H}$  NMR. Compound **30** (L=D) has not been synthesized before and so  $^{13}\text{C}$  and  $^1\text{H}$  NMR data have been included in the appendix.

## NMR analysis

All NMRs were taken in  $d_6$  benzene. The extent of deuterium/hydrogen incorporation was studied by integrating the quartet at  $\delta$  4.47 of the transferred proton against the two aromatic protons at  $\delta$  7.5. The aromatic protons in the standard reaction are set to 2.00 and the integration of quartet in the standard is considered to be the value, if no exchange occurred. The deuterium and hydrogen incorporation is estimated relative to the integrations of the standard reaction. All reactions are worked up at exactly the same time, though this was not really necessary (as described below).

The  $^1\text{H}$  NMR shifts for the non-transferred proton remaining at the benzylic position is  $\delta$  8.48 in  $\text{CDCl}_3$ . The relative integrations of this proton, when integrated against two aromatic protons at  $\delta$  7.82, in the standard v/s deuterium incorporation experiments for all three amines, were found to be the same. Since no deuterium incorporation is observed at this position an assumption is made that the reaction is irreversible. Hence one can assume that deuterium incorporation does not change with time and percent conversion.

## 6.4 Experimental Procedures for ‘Dynamic Effects in the Roush Allylboration of Aldehydes’

### General Procedure for the Allylboration of Aromatic Aldehydes using **43**

The Roush ester **43** was synthesized using literature procedures.<sup>51</sup> A solution containing 0.284 g (1 mmol) of **43** in 8 mL of dichloromethane was cooled in a dry ice-acetone bath and maintained at  $-78^\circ\text{C}$ . To this solution was added 0.151 g (1 mmol) of



**44a**. The reaction mixture was stirred for 30-60 min before the reaction was quenched by the addition of 10 mL of 0.1 N NaOH and 30 mL of diethylether. This two phase mixture was stirred vigorously for 30 min at room temperature to hydrolyze the boronate protected alcohol to the homoallylic alcohol **45a**. The resulting mixture was extracted with three portions of 10 mL of diethylether, and the combined organic layers were dried over Na<sub>2</sub>SO<sub>4</sub>. The solvent was then removed under reduced pressure to afford 0.215 g of the crude product mixture. The product **45a** is then easily purified by column chromatography using dichloromethane as eluent and 0.185 g (96 % yield) of **45a** was isolated. The isolated products characterized by <sup>1</sup>H NMR, were found to be free of starting materials or any other impurities. An identical procedure was followed for the reaction of **44b** with a slightly increased (2 h) reaction time to ensure complete conversion of the less reactive **44b**. For KIE measurements, a scaled up analog (15 mmol scale) of the above mentioned procedure was used. Conversions were determined by the comparison of starting material and product peaks in the NMR spectrum of the crude reaction mixture. The absence of no visible side products and complete consumption of the limiting reagent were confirmed by <sup>1</sup>H NMR. As a particular example, for the reaction of **43** and **44a**, separate reactions were taken to 18 ± 2% conversion in **43** and 22 ± 2% conversion in **44a** by using limiting amounts of the other reagent. The <sup>13</sup>C isotopic composition of the two samples of **45a**, isolated from these two reactions was compared against each other in order to determine KIEs as described in Chapter IV.

## NMR measurements

All samples were prepared using a constant 295 mg of **45a/45b** in 5 mm NMR tubes filled to a constant height of 5.0 cm. The  $^{13}\text{C}$  spectra were recorded at 125.70 MHz using inverse gated decoupling, 56 s (**45a**) or 52.5 s (**45b**) delays (5 times  $T_1$ ) between calibrated  $\pi/2$  pulses, and a 5.0 s acquisition time to collect 181 248 (**45a**) points 195 312 (**45b**). Integrations were numerically determined using a constant integration region for each peak. A zero-order baseline correction was generally applied, but no first-order correction was applied. Six spectra were recorded for each sample of recovered **45a/45b**. The  $^{13}\text{C}$  integrations and KIE determination from these NMR spectra are provided in the appendix.

## 6.5 Experimental Procedures for ‘Mechanism of Mukaiyama Aldol Reaction’

### General procedure for $\text{TiCl}_4$ mediated reaction of **48** and **49**

To a mixture of 0.12 g (1.0 mmol) of **49**, 0.190 g (1.1 mmol) of **48**, and 4 mL of dichloromethane maintained at  $-78\text{ }^\circ\text{C}$ , was added 1.1 mL of a 1 M solution (1.1 mmol) of  $\text{TiCl}_4$  in dichloromethane. The reaction was stirred for 1 h at  $-78\text{ }^\circ\text{C}$  after which it was quenched by the addition of 10 mL of saturated aqueous sodium bicarbonate and extracted three times using 20-mL portions of diethylether. The organic layer was dried using anhydrous sodium sulfate and concentrated under reduced pressure to yield a product mixture containing ~80% of **50** and small amounts of an unknown side product (presumably the corresponding chloride of **50**) and **49**.

**Preparation of NMR samples for  $^{13}\text{C}$  and  $^2\text{H}$  KIE measurements of **49****

Using a scaled up analog (25 mmol of **49**) of the general procedure but with slight modifications described below, two separate reactions were taken to  $65\pm 2\%$  and  $75\pm 2\%$  conversion in **49** by using appropriate amounts of **48**. Depending on conversion, as monitored by  $^1\text{H}$  NMR, extra **48** was added to attain the desired conversion of **49**. Using a 9:1 mixture of hexanes/ethyl acetate as eluent, **49** was recovered by column chromatography. NMR samples for  $^{13}\text{C}$  KIE measurements were prepared using 300 mg of **49** in 5 mm NMR tubes made up to 5 cm with  $\text{CDCl}_3$ . NMR samples for  $^2\text{H}$  KIE measurements were prepared using 600 mg of **49** and the samples were made up to 5 cm with  $\text{CHCl}_3$ . The standard for both these NMR measurements were prepared using the respective amounts of **49** drawn from the same bottle used for the reaction but not subjected to the reaction conditions.

**Preparation of NMR samples for  $^{13}\text{C}$  KIE measurements of **48****

Using a scaled up analog (50 mmol of **48**) of the general procedure but with slight modifications described below, two separate reactions were taken to  $75 \pm 2\%$  conversion in **48** by using limiting amounts of **49** (4.5 g or 37.5 mmol). The unreacted **48** was then recovered as the hydrolyzed ketone (pinacolone) from the reaction mixture by heat distillation. The recovered pinacolone contained significant amounts of hexamethyldisiloxane which had a single peak in the  $^{13}\text{C}$  NMR spectrum at  $\sim 0$  ppm. The standard for the NMR measurements were prepared using the pinacolone formed from the quantitative aqueous hydrolysis of **48**, not subjected to the reaction conditions,

using 5% HCl in dichloromethane. In order to nullify the errors arising from the peak at 0 ppm this sample was spiked with appropriate amounts of hexamethyldisiloxane drawn from an authentic sample.

### Synthesis of partially deuterated **48**

By refluxing 20 g (200 mmol) of pinacolone with 3 equiv of D<sub>2</sub>SO<sub>4</sub> and 4 equiv of D<sub>2</sub>O ~80% deuterium was incorporated in the methyl group. This partially deuterated pinacolone was extracted into 200 mL of dichloromethane and 23.9 g (220 mmol) of trimethylsilyl chloride, 33.5 g (220 mmol) of 1,8-diazabicyclo[5.4.0]undec-7-ene (DBU) and 34 g (200 mmol) of silver nitrate (AgNO<sub>3</sub>) was added and the resulting mixture refluxed for 14 h. The reaction mixture was consecutively washed with 100 mL of 1% aqueous HCl and 200 mL of saturated sodium bicarbonate and then extracted three times into 300-mL portions of diethylether. The extract was dried with anhydrous sodium sulfate and concentrated under reduced pressure to yield a mixture of partially deuterated **48** and pinacolone. The mixture was distilled to yield **48** free of any pinacolone. The partially deuterated **48** was found to be a mixture of 55% pure *d*<sub>2</sub>-**48**, 37% *d*<sub>1</sub>-**48** and 8% of protio **48**.

### *k*<sub>H</sub>/*k*<sub>D</sub> measurement of **48**

Using a scaled up analog (2.5 mmol of **49**) of the general procedure but using a 100% excess of **48**, reactions were taken to 50% conversion of **48**. Two sets of side-by-side reactions, one using **48** and the other using partially labeled **48**, were run for 1h. <sup>1</sup>H

NMR analysis of the crude product mixture showed that it contained as the major product **50** (>90%) and trace amounts of unknown side product and some hydrolyzed **48**. The deuterium content in the methylene carbon of **50** obtained from the reaction of partially deuterated **48** was compared to that of **50** obtained from a reaction of 100 % protio **48** as standard. From the net deuterium content in **50** and percent conversion of **48** the H/D KIE was easily determined.

## CHAPTER VII

## CONCLUSION

This dissertation represents a cross-section of the wide-ranging research ideas currently studied in the Singleton group. All the examples discussed in the preceding chapters are combined experimental and theoretical studies. The results and conclusions presented emphasize the importance of such an approach in elucidating reaction mechanisms and understanding new dynamic effects. The successful application of VTST with the inclusion of multidimensional tunneling calculations using POLYRATE to predict KIEs is a significant advance in our group's methodology.

Quasiclassical corner-cutting in organocatalysis marks the beginning of our work on a new type of dynamic effect that we think is important in several general acid-base catalyzed reactions in the realm of both organic and enzymatic chemistry. The results presented in Chapter II represent the first experimental example of this phenomenon in a relevant organic reaction. The most probable mechanism for the proline catalyzed aldol reaction is a rate-limiting attack of the enamine on the carbonyl of the aldehyde accompanied by proton transfer from the carboxylic acid of the proline to the incipient alkoxide. The predicted KIEs for this mechanism based on TST and VTST with multidimensional tunneling do not fit our experimentally measured isotope effects. Quasiclassical trajectories initiated on the potential energy surface of this reaction show that reactive trajectories show pronounced corner cutting. Remarkably, the KIE

predictions based on the mean crossing point of these quasiclassical trajectories, along the transition state ridge, accurately predict the experimental isotope effects.

The effect of recrossing on experimental KIEs was investigated for the Roush allylboration reaction. A detailed theoretical study showed that the amount of recrossing depended on how early or late the transition state was along the reaction coordinate. Based on these calculational results, an experimental study of the Roush allylboration of aldehydes was designed. Comparison of the  $^{13}\text{C}$  KIEs of two aldehydes with different amounts of recrossing provided support to our hypothesis that the experimental KIEs for the system with more recrossing would deviate more from the predictions based on TST. Detailed analysis of VTST effects were also performed to make better predictions of the KIEs. While this reconciled the discrepancy in the KIEs of the system with lesser recrossing, the disparity in the system with more recrossing was still outside experimental error. We believe that this is another example of recrossing affecting experimental observations in ordinary organic reactions.

Labeling studies in the base catalyzed isomerization of fluorinated imines revealed an important role of dynamic effects in determining the product ratio observed in the reaction. This reaction was thought to occur via a concerted 1,3 proton transfer. Our studies disprove this mechanism. Finally, the mechanistic investigation of the Mukaiyama aldol reaction shows that this reaction is not as straightforward as the textbook mechanism suggests. We propose a two- $\text{TiCl}_4$  model involving electron transfer from the titanium enolate to the  $\text{TiCl}_4$  complexed aldehyde in the key step in this reaction. In conclusion, the study of these important aldol reactions has led to some

intriguing results and a possible direction for future research efforts in the Singleton group.



## REFERENCES

- (1) Singleton, D. A.; Thomas, A. A. *J. Am. Chem. Soc.* **1995**, *117*, 9357-9358.
- (2) (a) Frantz, D. E.; Singleton, D. A. *J. Am. Chem. Soc.* **2000**, *122*, 3288-3295. (b) Singleton, D. A.; Merrigan, S. R. *J. Am. Chem. Soc.* **2000**, *122*, 11035-11036. (c) Singleton, D. A.; Wang, Y.; Yang, H. W.; Romo, D. *Angew. Chem. Int. Ed.* **2002**, *41*, 1572-1575. (d) Nowlan, D. T., III; Singleton, D. A. *J. Am. Chem. Soc.* **2005**, *127*, 6190-6191. (e) Singleton, D. A.; Wang, Z. *J. Am. Chem. Soc.* **2005**, *127*, 6679-6685.
- (3) (a) Singleton, D. A.; Hang, C.; Szymanski, M. J.; Greenwald, E. E. *J. Am. Chem. Soc.* **2003**, *125*, 1176-1177. (b) Bekele, T.; Christian, C. F.; Lipton, M. A.; Singleton, D. A. *J. Am. Chem. Soc.* **2005**, *127*, 9216-9223. (c) Ussing, B. R.; Singleton, D. A. *J. Am. Chem. Soc.* **2005**, *127*, 2888-2899.
- (4) Eyring, H. *J. Chem. Phys.* **1935**, *3*, 107-115.
- (5) Oyola, Y.; Singleton, D. A. *J. Am. Chem. Soc.* **2009**, *131*, 3130-3131.
- (6) Singleton, D. A.; Szymanski, M. J. *J. Am. Chem. Soc.* **1999**, *121*, 9455-9456.
- (7) (a) Bigeleisen, J.; Mayer, M. G. *J. Chem. Phys.* **1947**, *15*, 261-267. (b) Wolfsberg, M. *Acc. Chem. Res.* **1972**, *5*, 225-233. Bigeleisen, J. *J. Chem. Phys.* **1949**, *17*, 675-678.
- (8) Bell, R. P. *The Tunnel Effect in Chemistry*; Chapman & Hall: London, 1980; pp 60-63.
- (9) (a) Truhlar, D. G.; Garrett, B. C. *Ann. Rev. Phys. Chem.* **1984**, *35*, 159-189. (b) Truhlar, D. G.; Garrett, B. C.; Klippenstein, S. J. *J. Phys. Chem.* **1996**, *100*, 12771 .
- (10) (a) Carpenter, B. K. *Angew. Chem. Int. Ed.* **1998**, *37*, 3340-3350. (b) Carpenter, B. K. *J. Phys. Org. Chem.* **2003**, *16*, 858-868.
- (11) (a) Carpenter, B. K. *J. Am. Chem. Soc.* **1985**, *107*, 5730-5732. (b) Carpenter, B. K. *J. Am. Chem. Soc.* **1995**, *117*, 6336-6344. (c) Carpenter, B. K. *J. Am. Chem. Soc.* **1996**, *118*, 10329-10330. (d) Reyes, M. B.; Carpenter, B. K. *J. Am. Chem. Soc.* **2000**, *122*, 10163-10176. (e) Reyes, M. B.; Lobkovsky, E. B.; Carpenter, B. K. *J. Am. Chem. Soc.* **2002**, *124*, 641-651. (f) Nummela, J. A.; Carpenter, B. K. *J. Am. Chem. Soc.* **2002**, *124*, 8512-8513. (g) Litovitz, A. E.; Keresztes, I.; Carpenter, B. K. *J. Am. Chem. Soc.* **2008**, *130*, 12085-12094.

- (12) (a) Doubleday, C., Jr.; Bolton, K.; Hase, W. L. *J. Am. Chem. Soc.* **1997**, *119*, 5251-5252. (b) Doubleday, C.; Nendel, M.; Houk, K. N.; Thweatt, D.; Page, M. *J. Am. Chem. Soc.* **1999**, (c) *121*, 4720-4721. Doubleday, C.; Suhrada, C. P.; Houk, K. N. *J. Am. Chem. Soc.* **2006**, *128*, 90-94.
- (13) (a) Kless, A.; Nendel, M.; Wilsey, S.; Houk, K. N. *J. Am. Chem. Soc.* **1999**, *121*, 4524-4525. (b) Debbert, S. L.; Carpenter, B. K.; Hrovat, D. A.; Borden, W. T. *J. Am. Chem. Soc.* **2002**, *124*, 7896-7897.
- (14) (a) Metiu, H.; Ross, J.; Silbey, R.; George, T. F. *J. Chem. Phys.* **1974**, *61*, 3200-3209. (b) Valtazanos, P.; Ruedenberg, K. *Theor. Chim. Acta* **1986**, *69*, 281-307. (c) Windus, T. L.; Gordon, M. S.; Burggraf, L. W.; Davis, L. P. *J. Am. Chem. Soc.* **1991**, *113*, 4356-4357. (d) Tachibana, A.; Okazaki, I.; Koizumi, M.; Hori, K.; Yamabe, T. *J. Am. Chem. Soc.* **1985**, *107*, 1190-1196. (e) Zhou, C.; Birney, D. M. *Org. Lett.* **2002**, *4*, 3279-3282. (f) Wei, H.; Hrovat, D. A.; Borden, W. T. *J. Am. Chem. Soc.* **2006**, *128*, 16676-16683.
- (15) Thomas, J. B.; Waas, J. R.; Harmata, M.; Singleton, D. A. *J. Am. Chem. Soc.* **2008**, *130*, 14544-14555.
- (16) (a) Caramella, P.; Quadrelli, P.; Toma, L. *J. Am. Chem. Soc.* **2002**, *124*, 1130-1131. (b) Toma, L.; Romano, S.; Quadrelli, P.; Caramella, P. *Tetrahedron Lett.* **2001**, *42*, 5077-5080.
- (17) (a) Celebi-Olcum, N.; Ess, D. H.; Aviyente, V.; Houk, K. N. *J. Org. Chem.* **2008**, *73*, 7472-7480. (b) Limanto, J.; Khuong, K. S.; Houk, K. N.; Snapper, M. L. *J. Am. Chem. Soc.* **2003**, *125*, 16310-16321.
- (18) For the application of variational transition state theory to isotope effects on surfaces involving symmetry breaking, see: Gonzalez-Lafont, A.; Moreno, M.; Lluch, J. M. *J. Am. Chem. Soc.* **2004**, *126*, 13089-13094.
- (19) Hase, W. L. *Science* **1994**, *266*, 998-1002.
- (20) Ussing, B. R.; Hang, C.; Singleton, D. A. *J. Am. Chem. Soc.* **2006**, *128*, 7594-7607.
- (21) (a) Marcus, R. A.; Rice, O. K. *J. Phys. Colloid Chem.* **1951**, *55*, 894. (b) Marcus, R. A. *J. Chem. Phys.* **1952**, *20*, 355-364.
- (22) Clary, D. C. *Science* **2008**, *321*, 789 - 791.

- (23) Kuppermann, A.; Kaye, J. A.; Dwyer, J. P. *Chem. Phys. Lett.* **1980**, *74*, 257-262 (b) Romelt, J. *Chem. Phys. Lett.* **1980**, *74*, 263-268.
- (24) Parr, C. A.; Polanyi, J. C.; Wong, W. H. *J. Chem. Phys.* **1973**, *58*, 5-20.
- (25) (a) Hartke, B.; Manz, J. *J. Am. Chem. Soc.* **1988**, *110*, 3063-3068. (b) Gertitschke, P. L.; Kiprof, P.; Manz, J. *J. Chem. Phys.* **1987**, *87*, 941-952.
- (26) (a) Hajos, Z. G.; Parrish, D. R. *J. Org. Chem.* **1974**, *39*, 1615-1621. (b) Eder, U.; Sauer, G.; Wiechert, R. *Angew. Chem. Int. Ed. Engl.* **1971**, *10*, 496-497.
- (27) List, B.; Lerner, R. A.; Barbas, C. F., III. *J. Am. Chem. Soc.* **2000**, *122*, 2395-2396.
- (28) Hoang, L.; Martin, H. J.; List, B. *Proc. Natl. Acad. Sci. U.S.A.* **2004**, *101*, 5839-5842.
- (29) Marquez, C.; Metzger, J. O. *Chem. Comm.* **2006**, 1539-1541.
- (30) Hoang, L.; Bahmanyar, S.; Houk, K. N.; List, B. *J. Am. Chem. Soc.* **2003**, *125*, 16-17.
- (31) Klusmann, M.; Iwamura, H.; Mathew, S. P.; Wells, D. H.; Pandya, U.; Armstrong, A.; Blackmond, D. G. *Nature* **2006**, *441*, 621 - 623.
- (32) Bahmanyar, S.; Houk, K. N.; Martin, H. J.; List, B. *J. Am. Chem. Soc.* **2003**, *125*, 2475-2479.
- (33) Seebach, D.; Beck, A. K.; Badine, D. M.; Limbach, M.; Eschenmoser, A.; Treasurywala, A. M.; Hobi, R.; Prikoszovich, W.; Linder, B. *Helv. Chim. Acta* **2007**, *90*, 425-471.
- (34) Singleton, D. A.; Schulmeier, B. E. *J. Am. Chem. Soc.* **1999**, *121*, 9313-9317.
- (35) Kawasaki, T.; Komai, T. *Polymer J.* **1983**, *15*, 743-751
- (36) Onsager, L. *J. Am. Chem. Soc.* **1936**, *58*, 1486-1493.
- (37) Tomasi, J.; Persico, M. *Chem. Rev.* **1994**, *94*, 2027-2094.
- (38) Bondi, A. *J. Phys. Chem.* **1964**, *68*, 441-451.

- (39) The calculations used the program QUIVER – Saunders, M.; Laidig, K. E.; Wolfsberg, M. *J. Am. Chem. Soc.* **1989**, *111*, 8989-8994. Frequencies were scaled by 0.9614 – Scott, A. P.; Radom, L. *J. Phys. Chem.* **1996**, *100*, 16502-16513).
- (40) Corchado, J. C.; Chuang, Y.-Y.; Coitino, E. L.; Truhlar, D. G. *GAUSSRATE*, version 9.5; University of Minnesota: Minneapolis, MN, 2007.
- (41) Corchado, J. C.; *POLYRATE*, version 9.5; University of Minnesota: Minneapolis, MN, 2007.
- (42) Gaussian 03, Revision E.01, M. J. Frisch, G. W. Trucks, H. B. Schlegel, G. E. Scuseria, M. A. Robb, J. R. Cheeseman, J. A. Montgomery, Jr., T. Vreven, K. N. Kudin, J. C. Burant, J. M. Millam, S. S. Iyengar, J. Tomasi, V. Barone, B. Mennucci, M. Cossi, G. Scalmani, N. Rega, G. A. Petersson, H. Nakatsuji, M. Hada, M. Ehara, K. Toyota, R. Fukuda, J. Hasegawa, M. Ishida, T. Nakajima, Y. Honda, O. Kitao, H. Nakai, M. Klene, X. Li, J. E. Knox, H. P. Hratchian, J. B. Cross, V. Bakken, C. Adamo, J. Jaramillo, R. Gomperts, R. E. Stratmann, O. Yazyev, A. J. Austin, R. Cammi, C. Pomelli, J. W. Ochterski, P. Y. Ayala, K. Morokuma, G. A. Voth, P. Salvador, J. J. Dannenberg, V. G. Zakrzewski, S. Dapprich, A. D. Daniels, M. C. Strain, O. Farkas, D. K. Malick, A. D. Rabuck, K. Raghavachari, J. B. Foresman, J. V. Ortiz, Q. Cui, A. G. Baboul, S. Clifford, J. Cioslowski, B. B. Stefanov, G. Liu, A. Liashenko, P. Piskorz, I. Komaromi, R. L. Martin, D. J. Fox, T. Keith, M. A. Al-Laham, C. Y. Peng, A. Nanayakkara, M. Challacombe, P. M. W. Gill, B. Johnson, W. Chen, M. W. Wong, C. Gonzalez, and J. A. Pople, Gaussian, Inc., Wallingford CT, 2004.
- (43) See the Appendix for a complete description of the calculational methods employed.
- (44) Toney, M. D.; Kirsch, J. F. *Biochemistry* **1993**, *32*, 1471-1479
- (45) (a) Martell, A. E. *Acc. Chem. Res.* **1989**, *22*, 115-124. (b) Longenecker, J. B.; Snell, E. E. *J. Am. Chem. Soc.* **1957**, *79*, 142-145. (c) Casella, L.; Gullotti, M. *J. Am. Chem. Soc.* **1983**, *105*, 803-809. (d) Liu, L.; Rozenman, M.; Breslow, R. *J. Am. Chem. Soc.* **2002**, *124*, 12660-12661. (e) Liu, L.; Breslow, R. *J. Am. Chem. Soc.* **2002**, *124*, 4978-4979. (f) Breslow, R.; Canary, J. W.; Varney, M.; Waddell, S. T.; Yang, D. *J. Am. Chem. Soc.* **1990**, *112*, 5212-5219. (g) Breslow, R.; Chmielewski, J.; Foley, D.; Johnson, B.; Kumabe, N.; Varney, M.; Mehra, R. *Tetrahedron* **1988**, *44*, 5515-5524.
- (46) Jaeger, D. A.; Cram, D. J. *J. Am. Chem. Soc.* **1971**, *93*, 5153-5161

- (47) (a) Soloshonok, V. A.; Kirilenko, A. G.; Kukhar, V. P.; Resnati, G. *Tetrahedron Lett.* **1994**, *35*, 3119-3122. (b) Berbasov, D. O.; Ojemaye, I. D.; Soloshonok V. A. *J. Fluor. Chem.* **2004**, *125*, 603-607.
- (48) Ono, T.; Kukhar, V. P.; Soloshonok, V. A. *J. Org. Chem.* **1996**, *61*, 6563-6569.
- (49) (a) Soloshonok, V. A.; Ono, T. *J. Org. Chem.* **1997**, *62*, 3030-3031. (b) Soloshonok, V. A.; Ono T.; Soloshonok, I. V. *J. Org. Chem.* **1997**, *62*, 7538-7539. (c) Soloshonok, V. A.; Kirilenko, A. G.; Galushko, S. V.; Kukhar, V. P. *Tetrahedron Lett.* **1994**, *35*, 5063-5064. (d) Soloshonok, V. A.; Soloshonok, I. V.; Kukhar, V. P.; Svedas, V. K. *J. Org. Chem.* **1998**, *63*, 1878-1884. (e) Soloshonok, V. A.; Ohkura, H.; Yasumoto, M. *J. Fluor. Chem.* **2006**, *127*, 924-929. (f) Soloshonok, V. A.; Ohkura, H.; Yasumoto, M. *J. Fluor. Chem.* **2006**, *127*, 930-935.
- (50) Eyring, H. *Rev. Mod. Phys.* **1962**, *34*, 616 – 619.
- (51) (a) Roush, W. R.; Walts, A. E.; Hoong, L. K. *J. Am. Chem. Soc.* **1985**, *107*, 8186-8190. (b) Roush, W. R.; Park, J. C. *Tetrahedron Lett.* **1991**, *32*, 6285-6288. (c) Hoffmann, R. W.; Landmann, B. *Chem. Ber.-Recl.* **1986**, *119*, 1039. (d) Brown, H. C.; Bhat, K. S.; Randad, R. S. *J. Org. Chem.* **1987**, *52*, 319-320. (e) Brown, H. C.; Randad, R. S.; Bhat, K. S.; Zaidlewicz, M.; Racherla, U. S. *J. Am. Chem. Soc.* **1990**, *112*, 2389-2392. (f) Short, R. P.; Masamune, S. *J. Am. Chem. Soc.* **1989**, *111*, 1892-1894. (g) Corey, E. J.; Yu, C. M.; Kim, S. S. *J. Am. Chem. Soc.* **1989**, *111*, 5495-5496.
- (52) Roush, W. R.; Banfi, L.; Park, J. C.; Hoong, L. K. *Tetrahedron Lett.* **1989**, *30*, 6457-6460.
- (53) Gajewski, J. J.; Bocian, W.; Brichford, N. L.; Henderson, J. L. *J. Org. Chem.* **2002**, *67*, 4236-4240.
- (54) (a) Li, Y.; Houk, K. N. *J. Am. Chem. Soc.* **1989**, *111*, 1236-1240. (b) Vulpetti, A.; Gardner, M.; Gennari, C.; Bernardi, A.; Goodman, J. M.; Paterson, I. *J. Org. Chem.* **1993**, *58*, 1711-1718. (c) Gung, B. W.; Xue, X. W. *Tetrahedron: Asymmetry* **2001**, *12*, 2955-2959. (d) Omoto, K.; Fujimoto, H. *J. Org. Chem.* **1998**, *63*, 8331-8336.
- (55) Becke, A. D. *J. Chem. Phys.* **1993**, *98*, 5648-5652.
- (56) Lynch, B. J.; Fast, P. L.; Harris, M.; Truhlar, D. G. *J. Phys. Chem. A* **2000**, *104*, 4811-4815.
- (57) Doubleday, C., Jr.; Bolton, K.; Hase, W. L. *J. Phys. Chem. A* **1998**, *102*, 3648-3658.

- (58) Gilbert, T. M. *J. Phys. Chem. A*, **2004**, *108* (13), 2550–2554.
- (59) Kelly, K. K.; Hirschi, J. S.; Singleton, D. A. *J. Am. Chem. Soc.* **2009**, *131*, 8382–8383.
- (60) (a) Frantz, D. E.; Singleton, D. A.; Snyder, J. P. *J. Am. Chem. Soc.* **1997**, *119*, 3385–3386.
- (61) Mukaiyama, T.; Narasaka, K.; Banno, K. *Chem. Lett.* **1973**, 1011–1014.
- (62) Mukaiyama, T.; Banno, K.; Narasaka, K. *J. Am. Chem. Soc.* **1974**, *96*, 7503–7509.
- (63) Selected publication based on lewis acids used include (a) Kobayashi, S.; Uchiro, H.; Fujishita, Y.; Shiina, I.; Mukaiyama, T. *J. Am. Chem. Soc.* **1991**, *113*, 4247–4252. (b) Kobayashi, S.; Uchiro, H.; Shiina, I.; Mukaiyama, T. *Chem. Lett.* **1990**, *19*, 129–132. (c) Furuta, K.; Maruyama, T.; Yamamoto, H. *J. Am. Chem. Soc.* **1991**, *113*, 1041–1042. (d) Mikami, K.; Matsukawa, S. *J. Am. Chem. Soc.* **1994**, *116*, 4077–4078. (e) Ishitani, H.; Yamashita, Y.; Shimizu, H.; Kobayashi, S. *J. Am. Chem. Soc.* **2000**, *122*, 5403–5404. (f) Evans, D. A.; Murry, J. A.; Kozlowski, M. C. *J. Am. Chem. Soc.* **1996**, *118*, 5814–5815.
- (64) Mukaiyama, T.; Narasaka, K.; Banno, K. *Chem. Lett.* **1973**, *2*, 323–326.
- (65) Mukaiyama, T.; Saigo, K. *Chem. Lett.* **1973**, *2*, 479–482.
- (66) Zimmerman, H. E.; Traxler, M. D. *J. Am. Chem. Soc.* **1957**, *79*, 1920–1923.
- (67) Heathcock, C. H.; Davidsen, S. K.; Hug, K. T.; Flippin, L. A. *J. Org. Chem.* **1986**, *51*, 3027–3037 and references cited therein.
- (68) (a) Chan, T. H.; Aida, T.; Lau, P. W. K.; Gorys, V.; Harpp, D. N. *Tetrahedron Lett.* **1985**, *42*, 4029–4032. (b) Chan, T. H.; Brook, M. A.; *Tetrahedron Lett.* **1985**, *26*, 2943–2946. (c) Reetz, M. T.; Raguse, B.; Marth, C. F.; Huegel, H. M.; Bach, T.; Fox, D. N. A. *Tetrahedron* **1992**, *48*, 5731. (d) Yamago, S.; Machii, D.; Nakamura, E. *J. Org. Chem.* **1991**, *56*, 2098–2106. (e) Cozzi, P. G.; Floriani, C. *Organometallics* **1994**, *13*, 2131. (f)
- (69) (a) Heathcock, C.H.; Hug, K.; Flippin, L. A. *Tet.Lett.* **1984**, *25*, 5973 –5976 (b) Heathcock, C. H.; Davidsen, S.; Hug, K.; Flippin, L. A. *J. Org. Chem.* **1986**, *51*, 3027–3037 (c) Heathcock, C.H.; Flippin, L. *J. Am. Chem. Soc.* **1983**, *105*, 1667 – 1668.
- (70) Denmark, S. E.; Lee, W. *J. Org. Chem.* **1994**, *59*, 707–709.

- (71) Wong, C. T.; Wong, M. W. *J. Org. Chem.* **2007**, *72*, 1425-1430.
- (72) Dolg, M.; Stoll, H.; Preuss, H.; Pitzer, R. M. *J. Phys. Chem.* **1993**, *97*, 5852-5859.
- (73) Sato, T.; Wakahara, Y.; Otera, J.; Nozaki, H. *J. Am. Chem. Soc.* **1991**, *113*, 4028-4030.
- (74) Nakamura, E.; Kuwajima, I. *Tett. Lett.* **1984**, *24*, 3343-3346.
- (75) (a) Gajewski, J. J.; Bocian, W.; Harris, N. J.; Olson, L. P.; Gajewski, J. P. *J. Am. Chem. Soc.* **1999**, *121*, 326-334. (b) Yamataka, H.; Matsuyama, T.; Hanafusa, T. *J. Am. Chem. Soc.* **1989**, *111*, 4912-4918.
- (76) Mahrwald, R. *Chem. Rev.* **1999**, *99*, 1095-1120.
- (77) [http://comp.chem.umn.edu/gaussrate/gaussrate\\_Manual\\_v2008.2009.5.11.pdf](http://comp.chem.umn.edu/gaussrate/gaussrate_Manual_v2008.2009.5.11.pdf)

## VITA

Name	Mathew J. Veticatt
Address	26 Bayberry Lane Rye Brook, NY 10573
Email address	mjvcatt@gmail.com
Education	B.Tech., Technology of Oils, Surfactants and Oleochemicals, Mumbai University Institute of Chemical Technology (2005)  Ph.D., Chemistry, Texas A&M University (2009)